Anderson Localization as a Percolation Transition

BY

Lorenzo Tonetti

Submitted for the

Master's Degree in Physics of Complex Systems
(International Track)

Supervisor:
Prof. Alfredo Braunstein

External supervisors:
Prof. Leticia F. Cugliandolo,
Prof. Marco Tarzia

Politecnico di Torino
ACADEMIC YEAR 2024-2025

Abstract

Anderson localization is a fundamental phenomenon in condensed matter physics that describes the suppression of wave propagation due to disorder-induced interference effects. The Bethe lattice solution is the only known exact solution to the Anderson localization problem. A recent proposal by Filoche and Mayboroda claims to predict the position of the mobility edge in Anderson localization for systems in finite dimensions. This framework, that they called “Localization Landscape Theory", introduces a function called localization landscape whose inverse acts as an effective potential, identifying regions where quantum states are spatially confined. The main claim of Filoche and Mayboroda’s work is that the Anderson transition occurs when the regions with effective potential energy lower than the eigenstate energy percolate through the lattice—thus interpreting Anderson localization as a percolation transition. In this work we derive and solve numerically the equations determining the transition according to the localization landscape percolation on the Bethe lattice, showing that this framework is not able to reproduce the critical properties of Anderson localization on a generic lattice.

Contents

Introduction

Anderson localization is a fundamental phenomenon in condensed matter physics, first predicted by P.W. Anderson in 1958 [1]. It describes how wave propagation can be suppressed due to disorder. For electronic transport in disordered media, interference between multiple scattering paths can completely localize electronic wavefunctions, preventing transport. This effect is particularly strong in low-dimensional systems, where even infinitesimal disorder may localize all eigenstates. The transition between localized and extended states is characterized by a critical curve in parameter space called the mobility edge, which separates insulating and conducting behaviors [2].

Anderson localization has been observed in various physical systems [2]. For instance, ultrasound waves can localize in elastic networks [3], and electromagnetic waves in disordered crystalline lattices [4].

Research on Anderson localization has extensively examined the tight-binding model on Bethe lattices, where exact solutions provide insights into localization properties of real disordered materials [5–8]. The density of states and mobility edge dependence on disorder strength have been analyzed using techniques like the cavity method [9] and population dynamics [10].

The “Localization Landscape Theory", introduced by M. Filoche and S. Mayboroda in 2012 [11], provides a method to predict the spatial distribution of localized states in quantum disordered systems without directly solving the Schrödinger equation. The theory introduces a localization landscape $u(\mathbf{x})$. In the tight-binding approximation, this landscape takes a discretized form $\mathbf{u}$, represented in the occupation number basis where states are indexed by electron occupancy at each site. Each component u_i corresponds to a lattice site i. The localization landscape satisfies a differential equation similar to the Schrödinger equation but with a uniform right-hand side, which in the occupation number basis reads

$$\hat{\mathcal{H}}\mathbf{u} = \mathbf{1}, \tag{1}$$

where $\hat{\mathcal{H}}$ is the Hamiltonian operator and $\mathbf{1}$ is a vector with all entries equal to 1. Section 1.4 will briefly outline the derivation of this theory.

A central claim of [11] is that this framework provides a way to predict the spatial distribution of localized states using effective potentials $1/u_i$. The crests of the effective potential define confinement regions for eigenstates, offering a way to understand localization without explicit eigenfunction computation. According to this proposal, the sets of nearest-neighboring sites with effective potential below E, determine the regions of the lattice where an electron with energy E is classically confined. If a macroscopic (“giant") cluster of this kind exists, electrons could classically percolate through the lattice, indicating that the system is in the delocalized phase.

To date, the Localization Landscape Theory has only been tested numerically for the Anderson model on a cubic lattice of limited size ($N = 50$), leaving uncertainties due to finite-size effects [12]. For this reason the aim of this work has been to derive

and solve numerically the equations determining the critical properties of the localization landscape percolation problem for the Anderson model on the only lattice where the exact solution of Anderson localization is known, i.e. the Bethe lattice. The aim was to put the Localization Landscape Theory to the test and characterize its possible limits of validity.

In Sec. 1, after summarizing some fundamental results about Anderson localization and percolation theory, we present a sketch of the derivation of Localization Landscape Theory for the discrete lattice case. In Sec. 2.1 we derive the equations for the localization landscape $\mathbf{u}$ on the Bethe lattice. Sections 2.2 and 2.3 contain our derivation of the equations that determine the critical properties of the localization landscape percolation problem and of Anderson localization on the Bethe lattice. We then provide in Sec. 3 important analytical results derived from these equations in the high-connectivity limit. Finally, Sec. 4 compares these results of Anderson localization's critical properties with those from the "Localization Landscape Theory", in order to evaluate how well the theory predicts the actual Anderson critical properties.

Chapter 1

Preliminaries

In this section we summarize some important definitions and results that will be useful later.

1.1 Random Regular Graphs

Random regular graphs are an important class of random graphs in which each node has exactly the same degree $K+1$, ensuring uniform connectivity across the network. They are random in the sense that a random regular graph with N vertices is a graph drawn uniformly from the set of all the graphs with N nodes and fixed degree [13, 14]. These graphs serve as useful models of space in statistical physics since in the thermodynamic limit they represent the infinite dimensional limit for Euclidean lattices, while preserving a finite local connectivity. In contrast, the usual mean-field approximation performed making the graph fully connected, has infinite connectivity in the thermodynamic limit, and loses the notion of distance, since all pairs of sites are connected by a path of length 1. Moreover, for the Anderson localization problem one cannot observe the localization transition in the fully-connected geometry [15].

An important feature of random regular graphs is that they are locally tree-like. In fact, it can be shown that the typical size of loops grows as $\ln N/\ln K$, and this implies that, asymptotically, systems defined on a random regular graph are well described by their behavior on a Bethe lattice, i.e. an infinite tree with fixed connectivity [13, 14]. The most important properties of the Bethe lattice, which add to the ones of the random regular graph, are the ones descending from its infinite-tree structure:

- It is translational invariant,
- Conditioning on one of the vertices, the $K+1$ branches of the remaining graph become statistically independent [16],
- There is only one simple path between two vertices.

These properties simplify the analytic calculations needed to find equations for the critical behavior.

1.2 Anderson Localization

Anderson localization was originally studied in the context of electronic transport, but has since been observed in many other condensed matter systems [2–4]. This phenomenon occurs when disorder in a system leads to the suppression of wave

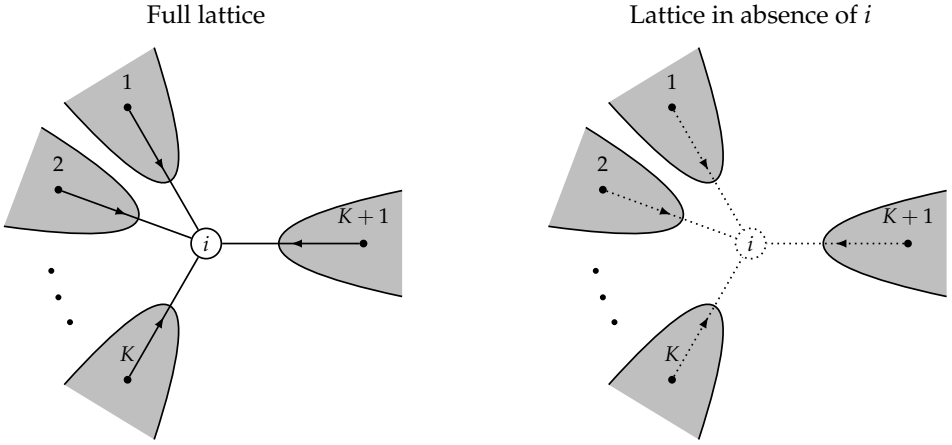

FIGURE 1.1: Left: schematic representation of a Bethe lattice (centered on a reference site i), i.e. an infinite tree with fixed coordination number $K+1$. The grey regions indicate the subtrees rooted at the nearest neighbors of i. Right: representation of the same structure with site i removed. After removing the edge connecting i to a given subtree, the disconnected subtree is itself an infinite tree with the same coordination number $K+1$, except at the root (the nearest neighbor of i), which has coordination K. Under the assumption that site-dependent quantities depend explicitly only on the nearest neighbors, conditioning on site i makes the neighboring subtrees statistically independent. This follows directly from the global Markov property of factor graphs [16]. These decoupled subtrees are referred to as cavity subtrees, or cavity lattices. Conditioning on a site thus allows one to express local observables on the Bethe lattice in terms of conditionally independent quantities defined at the roots of the cavity lattices.

propagation. In particular, for electronic transport it can be explained as the transition of the eigenstates of the electronic Hamiltonian from being extended, i.e. having non-zero amplitude on the whole lattice, to being localized on particular sites, i.e. having exponentially decaying amplitude with the distance from a site. The effect arises from the interference between multiple scattering paths in the disordered potential, which can completely inhibit electronic transport and turn what would normally be a conducting material into an insulator [2]. One of the most important models in the description of Anderson localization is the tight binding Anderson model [1], the Hamiltonian of which reads

$$\hat{\mathcal{H}} = \sum_i \epsilon_i \hat{c}_i^\dagger \hat{c}_i - t \sum_{\langle i,j \rangle} \left(\hat{c}_i^\dagger \hat{c}_j + \hat{c}_j^\dagger \hat{c}_i \right) = \sum_i \epsilon_i |i\rangle\langle i| - t \sum_{\langle i,j \rangle} \left(|i\rangle\langle j| + |j\rangle\langle i| \right), \tag{1.1}$$

where $\hat{c}_i^\dagger$ and $\hat{c}_i$ are the creation and annihilation operators at site i in the second-quantization formalism (the kets $|i\rangle$, in the first-quantization representation, identify the quantum states where an electron is localized on a site i), ϵ_i is the on-site disorder potential, drawn from the uniform distribution

$$\gamma_s(\epsilon) = \begin{cases} 1/W & \text{if } \epsilon \in [-W/2, W/2], \\ 0 & \text{else,} \end{cases} \tag{1.2}$$

t is the hopping amplitude between neighboring sites, and $\sum_{\langle i,j \rangle}$ denotes the sum over nearest-neighboring pairs. A key mathematical tool for analyzing localization

properties is the resolvent (or Green's function), defined as

$$\hat{\mathcal{G}}(z) = (z\mathbb{I} - \hat{\mathcal{H}})^{-1}, \tag{1.3}$$

where $\hat{\mathcal{H}}$ is the Hamiltonian of the system, and $z = E - \mathrm{i}\alpha$ is a complex number whose imaginary part is useful for regularization reasons. The imaginary part of the diagonal elements of $\hat{\mathcal{G}}(z)$, i.e.

$$\mathcal{G}_{ii}(z) = \langle i|\hat{\mathcal{G}}(z)|i\rangle\,, \tag{1.4}$$

is directly related to the local density of states, while its decay properties characterize the spatial extent of wavefunctions. The local density of states at site i and energy E is given in terms of the imaginary part of the Green's function as

$$\rho_i(E) = \sum_n |\psi_i^{(n)}|^2 \delta(E - E_n) = \frac{1}{\pi}\mathrm{Im}\,\mathcal{G}_{ii}(E - \mathrm{i}0^+), \tag{1.5}$$

where $\mathcal{G}_{ii}(E - \mathrm{i}\alpha)$ is the diagonal element of the advanced Green's function (the distiction between "advanced" and "retarderd" Green's functions comes from the choice of $z = E \pm \mathrm{i}\alpha$ with $\alpha > 0$ in Eq. (1.3)). The expression of ρ_i in terms of $\mathcal{G}_{ii}$ is a well-known result, and the derivation can be found in Ref. [17].

The local densities of states are the key parameters needed to identify the transition, since in the localized phase $\rho_i(E)$ is exponentially small in $O(N)$ sites, and of $O(1)$ in $O(1)$ sites, while in the delocalized phase $\rho_i(E)$ is non-zero on $O(N)$ sites, allowing for transport. Another important order parameter for the transition is the "Inverse Participation Ratio" or IPR, which is defined as

$$I_2(E) = \mathbb{E}\left[\frac{\sum_n \sum_i |\psi_i^{(n)}|^4 \delta(E_n - E)}{\sum_n \delta(E_n - E)}\right] = \mathbb{E}\left[\lim_{\alpha\to 0^+} \frac{\alpha \sum_i |\mathcal{G}_{ii}(E - \mathrm{i}\alpha)|^2}{\sum_i \mathrm{Im}\,\mathcal{G}_{ii}(E - \mathrm{i}\alpha)}\right], \tag{1.6}$$

and is essentially a measure of the average inverse volume occupied by an eigenstate. In the delocalized phase $I_2(E) \sim O(1/N)$, while in the localized one $I_2(E) \sim O(1)$. Finally, the last quantity that we are interested in is the eigenstate correlation function, which is defined as

$$C_{loc}(|i-j|\,; E) = \mathbb{E}\left[\frac{\sum_n |\psi_i^{(n)}|^2 |\psi_j^{(n)}|^2 \delta(E_n - E)}{\sum_n \delta(E_n - E)}\right] = \mathbb{E}\left[\lim_{\alpha\to 0^+} \frac{\alpha |\mathcal{G}_{ij}(E - \mathrm{i}\alpha)|^2}{\sum_i \mathrm{Im}\,\mathcal{G}_{ii}(E - \mathrm{i}\alpha)}\right], \tag{1.7}$$

and it represents the average correlation between the amplitude of an eigenstates on two sites at distance $|i - j|$. The expectation values in Eqs. (1.6),(1.7) are taken over the disorder variables ϵ_i. The algebraic steps leading to the final expression in Eq. (1.6) are detailed in Ref. [18], and the last term in Eq. (1.7) is derived in an analogous way. From Eqs. (1.5),(1.6),(1.7) it is evident that the critical properties of Anderson localization on a generic lattice are fully determined by $\hat{\mathcal{G}}(z)$. The advantage of working with the Bethe lattice is that the computation of the components of $\mathcal{G}_{ij}(z)$ is much simpler thanks to the cavity method. The final result for the diagonal elements is

$$\mathcal{G}_{ii}(z) = \frac{1}{z - \epsilon_i - t^2 \sum_{k\in\partial i} \mathcal{G}_{k\to i}(z)}, \tag{1.8}$$

where the symbol ∂i represents the set of nearest neighbors of site i, and the terms

$\mathcal{G}_{i\to j}(z)$ are the cavity Green's functions on site i in the absence of site j. They satisfy an analogous recursion relation, which is the so-called cavity equation for the Green's function:

$$\mathcal{G}_{i\to j}(z) = \frac{1}{z - \epsilon_i - t^2 \sum_{k\in\partial i\setminus j} \mathcal{G}_{k\to i}(z)}, \tag{1.9}$$

where $\partial i\setminus j$ is a shorthand notation for $\partial i\setminus\{j\}$ and "\" is the symbol of difference between sets. The derivation of Eqs. (1.8) and (1.9) is very similar to the one that we will present in Sec. 2.1, and can be found in Ref. [6].

The most important quantity determining the position of the mobility edge is the imaginary part of the Green's function, entering in the local density of states. The interpretation of the real part of the Green's function has remained elusive. The "Localization Landscape Theory" could give it an interpretation. In fact, as we will show in Sec. 2.1, the localization landscape $\mathbf{u}$ is directly related to $\mathrm{Re}[\mathcal{G}_{ii}(2t\sqrt{K} + W/2 - \mathrm{i}\alpha)]$.

1.3 Percolation on the Bethe lattice

Percolation is a fundamental physical phenomenon describing the formation of connected regions (or "clusters") in a disordered medium as a function of increasing connectivity. In everyday life, a simple example of percolation is the flow of water inside a coffee filter. Depending on the structure of available paths inside the filter, the water will either be able to percolate through the material, seeping from one side to the other, or end up stuck in a "non-percolating path".

This effect can be described using many mathematical models. This rich theoretical framework is known as percolation theory [19]. Applications of percolation theory comprehend: percolation of particles through membranes in chemistry and biology [20, 21], contact networks in epidemiology [22, 23], and as we have anticipated in the introduction, electronic transport in disordered media [12].

In the most general case the percolation model is defined on a graph $G = (V, E)$. Here V is the set of N "vertices" (or "sites") and E is the set of "edges" (or "bonds") of the graph. The two classical models for percolation are:

- Site percolation: We consider a graph where all the bonds in the set E are active but the sites can be "occupied" or "not occupied", independently, with probabilities q or $1 - q$;
- Bond percolation: In a similar way, one considers that all the sites as occupied, and takes each bond in E to be "active" with probability q or "inactive" with probability $1 - q$.

In both models a path in the graph is defined as a set of active bonds connecting occupied sites. A set of all occupied sites connected by a path is called a cluster, and the "size" of a cluster is defined as the number of sites that it contains. In the thermodynamic limit, as q increases past a critical threshold q_c (different for the 2 percolation types), a "giant" (i.e. containing $O(N)$ sites) cluster appears, allowing long-range transport, i.e. the existence of a path "from one side to the other" of the graph. Below q_c, only small, finite clusters exist. The percolation transition is a "phase transition", but unlike conventional statistical physics phase transitions, it does not rely on an underlying Hamiltonian, making its critical behavior an interesting subject of study of pure geometric origin.

The percolation problem can be slightly modified by considering both site occupation and bond activation as random, creating a site-bond percolation problem. In

order to apply the results of percolation theory in a more flexible way to the Anderson localization problem, we start by obtaining the site-bond percolation critical curve in terms of the independent control parameters q and q_B. The fundamental quantities for this problem are defined as

$$q = \Pr\{O_i = 1\}\,, \quad q_B = \Pr\{A_{i,j} = 1\}, \tag{1.10}$$

$$p(q, q_B) = \Pr\{\text{site } i \text{ belongs to the giant cluster}\}, \tag{1.11}$$

where

$$O_i = \begin{cases} 1 & \text{if site } i \text{ is occupied} \\ 0 & \text{else} \end{cases} \qquad A_{i,j} = \begin{cases} 1 & \text{if bond } (i,j) \text{ is active} \\ 0 & \text{else} \end{cases} \tag{1.12}$$

On the Bethe lattice $p(q, q_B)$ should be translational invariant, and thus independent of the particular site. This quantity can be computed recursively on the graph as follows:

$$\begin{aligned} p(q, q_B) &= q \Pr\left\{\exists j \in \partial i \text{ in the giant cluster}, A_{i,j} = 1\right\} = \\ &= q \sum_{l=1}^{K+1} \underbrace{\Pr\left\{A_{i,j_k} = 1 \text{ for at least a } k \in \{1,\dots,l\}\right\}}_{[1-(1-q_B)^l]} \underbrace{\Pr\left\{\{j_1,\dots,j_l\} \in \partial i \text{ are in the infinite cluster}\right\}}_{\binom{K+1}{l} p_{cav}(q,q_B)^l [1-p_{cav}(q,q_B)]^{K+1-l}}, \\ &= q\left[1 - (1 - p_{cav}(q, q_B) q_B)^{K+1}\right], \end{aligned} \tag{1.13}$$

where ∂i is the set of nearest neighbors of i, and $p_{cav}(q, q_B)$ is the cavity percolation probability, and it is defined in the same way as $p(q, q_B)$ but on a lattice where one of the branches connected to site i has been removed. As mentioned in the caption of Fig. 1.1, this modified lattice (one of the subtrees in the right image of this figure) is the so-called cavity lattice. The cavity percolation probability can be computed in an analogous way, i.e.

$$p_{cav}(q, q_B) = q[1 - (1 - p_{cav}(q, q_B) q_B)^K]. \tag{1.14}$$

The percolation transition occurs when the solution of this recursive equation becomes non-zero. This means that we can find the expression for the critical curve in the plane (q, q_B) by expanding the right-hand-side of Eq. (1.14) for p_{cav} small. The result is

$$q q_B = 1/K, \tag{1.15}$$

in analogy with the critical threshold for site percolation on the Bethe lattice [19] with occupation probability $q q_B$. The critical curve is a hyperbola and is symmetric in the exchange of q and q_B even though the cavity equation (1.14) is not. Two quantities that will be useful later to describe the percolation transition described by the localization landscape framework will be the two-point correlation function, and the average cluster size.

The correlation function $C_p(r)$ for a percolation problem on the Bethe lattice is defined as the probability that two sites at distance r belong to the same cluster. Denoting as $0, \dots, r$ the sites along a simple path of length r on the lattice we have

$$C_p(r) \equiv \Pr\{O_0 = 1, A_{0,1} = 1, \dots, A_{r-1,r} = 1, O_r = 1\}\,. \tag{1.16}$$

The average cluster size S represents the average size of the connected component in the lattice to which a generic occupied site belongs. This can be computed

directly from the correlation function, by observing that the average number of sites at distance r belonging to the same cluster as site i is $(K+1)K^{r-1}C_p(r)/q$ (the factor $1/q$ is needed to condition the probability on the occupation of the reference site). Therefore, the average number of sites belonging to the same cluster of site i, regardless of their distance, will be just

$$S = 1 + \sum_{r=1}^{\infty} (K+1)K^{r-1}\frac{C_p(r)}{q}. \tag{1.17}$$

Note that these two definitions are independent of the criterion that we choose for the site occupation (as long as q is defined as the probability of a generic site to be occupied). Therefore, they are completely general, and they can be used for any kind of correlated or uncorrelated percolation problem on the Bethe lattice. For the site-bond percolation problem the correlation function is just

$$C_p(r) = q(qq_B)^r = \frac{q}{K^r}e^{-r/\xi_p}, \tag{1.18}$$

with

$$\xi_p = -\frac{1}{\ln Kqq_B}, \tag{1.19}$$

which represents the correlation length of the problem, and as expected diverges at criticality as $\xi_p \sim |qq_B - 1/K|^{-\nu}$ (and $\nu = 1$). The average cluster size follows directly from Eq. (1.17), also diverges at criticality with a power law ($S \sim |qq_B - 1/K|^{-\gamma}$ with $\gamma = 1$), and reads

$$S = \frac{1 + qq_B}{1 - Kqq_B}. \tag{1.20}$$

1.4 "Localization Landscape Theory"

In this section we will summarize the main ideas and derivations of "Localization Landscape Theory" in the discrete lattice case. As we will see in Sec. 4 some of the hypothesis of this proposal will be contradicted by our results, but in the following we will describe the framework as it has been introduced in Refs. [11, 12, 24].

According to the latter references, the localization landscape defines regions where the eigenstates are confined, and the transition to delocalization can be understood as a "percolation" of the classically allowed regions throughout the system. Moreover, the inverse of the localization landscape represents an effective potential; therefore, electrons with energy E are classically confined to regions where $1/u_i < E$. The delocalization transition should then occur when the set of classically allowed sites $\Omega_E = \{i|1/u_i \leq E\}$ forms a connected path spanning the system. This percolation approach provides an alternative interpretation of the Anderson transition, where the mobility edge, traditionally understood as the energy separating localized and delocalized states, could be determined as the critical curve of this classical percolation problem.

The definition of the set Ω_E follows from the following argument. We start by defining the localization landscape $\mathbf{u}$ as the solution of Eq. (1). We want to show that the quantity $\widehat{1/u} \equiv \sum_i \frac{1}{u_i}|i\rangle\langle i|$ represent an effective potential. From now on we will work with a positive definite Hamiltonian to simplify calculations, but the result can be easily mapped to the case of the original Hamiltonian. In the usual Anderson tight-binding Hamiltonian the spectrum is symmetric, and it has been shown in Refs. [25, 26] that on the Bethe lattice the energies E take values in the interval $[-2t\sqrt{K} - W/2, 2t\sqrt{K} + W/2]$. So, in order to make $\hat{\mathcal{H}}$ positive definite we just need to translate all the random on-site energies ϵ_i by the fixed amount $2t\sqrt{K} + W/2$. After this translation, the spectrum of the Hamiltonian takes values in the interval $[0, 4t\sqrt{K} + W]$. The functional form of the Hamiltonian in Eq. (1.1) remains the same as long as we define the on-site energies as random variables $\varepsilon_i = \epsilon_i + 2t\sqrt{K} + W/2$, i.e. drawn uniformly from $[2t\sqrt{K}, 2t\sqrt{K} + W]$. Therefore, the probability distribution of the ε_i's is

$$\gamma(\varepsilon) = \gamma_s(\varepsilon - 2t\sqrt{K} - W/2) = \begin{cases} 1/W & \text{if } \varepsilon \in [2t\sqrt{K},\, 2t\sqrt{K} + W], \\ 0 & \text{else,} \end{cases} \tag{1.21}$$

where γ_s is the one in Eq. (1.2). Working now with this Hamiltonian, the equation that defines $\mathbf{u}$ can be written in terms of the Green's function as

$$\mathcal{G}^{-1}\mathbf{u} = \mathbf{1}. \tag{1.22}$$

The latter follows from Eq. (1) by defining $\mathcal{G} = \hat{\mathcal{H}}^{-1}$. Then, by multiplying on the left by $\mathcal{G}$ we obtain

$$u_i = \sum_j \mathcal{G}_{ij}. \tag{1.23}$$

Having translated the diagonal elements, the Hamiltonian now falls in the class of non-singular M-matrices. A non-singular M-matrix is defined as a non-singular real valued square matrix whose off-diagonal elements are non-positive, and whose inverse exists and is non-negative. The result known as "M-matrix eigenvalue criterion" states that if a non-singular real valued matrix has non-positive off-diagonal terms and all eigenvalues with positive real-parts then it is a non-singular M-matrix. For this reason, the Green's function exists and all its entries are non-negative. This

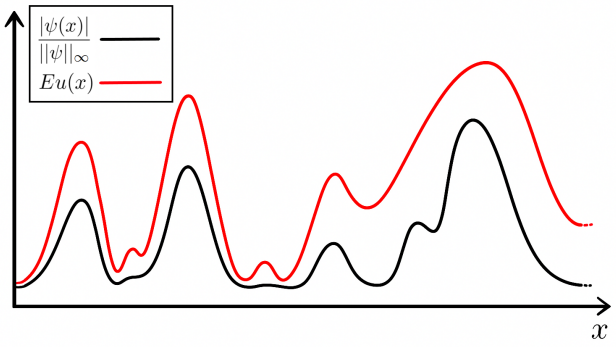

FIGURE 1.2: Sketch of the inequality of Eq. (1.26). The amplitude of all eigenfunctions is bounded by a quantity proportional to the localization landscape. Therefore, wherever the localization landscape is small the amplitude of the eigenfunctions must be small too, signaling that the valleys of the localization landscape should delimit the regions where the eigenfunctions have non-zero amplitude.

also implies that the components of $\mathbf{u}$ are all non-negative. Thus, summarizing

$$\mathcal{G}_{ij} \geq 0 \;\; \forall\, i,j \quad \text{and} \quad u_i \geq 0 \;\forall\, i. \tag{1.24}$$

A direct consequence of this is that we can find an equation to show that the eigenstates of the Hamiltonian are confined inside domains delimited by the valleys of the localization landscape $\mathbf{u}$. Now, let $|\psi\rangle$ be an eigenstate of the Hamiltonian with energy E (decomposed in the lattice sites basis as $|\psi\rangle = \sum_i \psi_i |i\rangle$). Using Eqs. (1.23),(1.24) we can write

$$\begin{aligned} |\psi_i| \equiv |\langle i|\psi\rangle| = |\langle i|\mathcal{H}^{-1}\mathcal{H}|\psi\rangle| = E\left|\langle i|\mathcal{H}^{-1}|\psi\rangle\right| = E\sum_j \underbrace{(\mathcal{H}^{-1})_{ij}}_{\mathcal{G}_{ij}\geq 0}|\psi_j| \\ \leq E\underbrace{\max_i |\psi_i|}_{||\psi_i||_\infty}\underbrace{\sum_j \mathcal{G}_{ij}}_{u_i} = Eu_i||\psi||_\infty. \end{aligned} \tag{1.25}$$

Thus,

$$\frac{|\psi_i|}{||\psi||_\infty} \leq Eu_i. \tag{1.26}$$

This equation is the discrete version of Eq. (3) in [11], and the derivation that we have shown is analogous to the one in the appendix of [11], with the only difference that in this case we work with discrete quantities. The direct consequence of Eq. (1.26) is that the amplitudes of the eigenfunctions are bounded by the localization landscape. Therefore, the eigenstates must be confined within the basins delimited by the valleys of the localization landscape (i.e. by the crests of the effective potential), as sketched in Fig. 1.2.

In the following we derive an equation that, according to [24] should explicitly highlight the role of $\widehat{1/u}$ as an effective potential:

$$\begin{aligned}\langle i|\hat{\mathcal{H}}|\psi\rangle &= (\hat{\mathcal{H}}\psi)_i = \varepsilon_i\psi_i - t\sum_{j\in\partial ii}\psi_j = (\varepsilon_i - t(K+1))\psi_i - t\sum_{j\in\partial i}(\psi_j-\psi_i)\\ &= \varphi_i\underbrace{\left[(\varepsilon_i - t(K+1))u_i - t\sum_{j\in\partial i}(u_j-u_i)\right]}_{(\hat{\mathcal{H}}\mathbf{u})_i=1} - t\sum_{j\in\partial i}u_j(\varphi_j-\varphi_i)\\ &= \varphi_i - t\sum_{j\in\partial i}u_j(\varphi_j-\varphi_i).\end{aligned} \tag{1.27}$$

In the second line we have introduced the variables $\varphi_i = \psi_i/u_i$, and we have added and subtracted $u_j\varphi_i$ to the expression. By definition, $\langle i|\hat{\mathcal{H}}|\psi\rangle = E\psi_i = Eu_i\varphi_i$, which means that

$$-t\sum_{j\in\partial i}\frac{u_j}{u_i}(\varphi_j-\varphi_i) + \frac{1}{u_i}\varphi_i = E\varphi_i. \tag{1.28}$$

This equation represents the discrete version of

$$-\frac{t}{u^2}\nabla\cdot(u^2\nabla\varphi) + \frac{1}{u}\varphi = E\varphi, \tag{1.29}$$

which is an equation of Schröedinger type for φ with potential $\widehat{1/u}$. It is the analog of Eq. (5) in [27]. The proof of the equivalence between Eqs. (1.28) and (1.29) is written in App. A. This equation tells us that $\widehat{1/u}$ is the potential for the Schröedinger equation of a modified wavefunction, and, as we argue in Sec. 4, this could break the interpretation that [12] uses to define the percolation problem. One last result that gives credit to the effective potential interpretation, is that the energy of any quantum state (not necessarily an eigenstate) is always greater or equal than the effective potential energy $\langle\psi|\widehat{1/u}|\psi\rangle$. In fact,

$$\begin{aligned}\langle\psi|\hat{\mathcal{H}}|\psi\rangle &= \sum_i\psi_i(\hat{\mathcal{H}}\psi)_i = \sum_i u_i\varphi_i^2 - t\sum_i\sum_{j\in\partial i}u_iu_j(\varphi_j-\varphi_i)\\ &= \sum_i u_i\varphi_i^2 - 2t\sum_{\langle i,j\rangle}u_iu_j(\varphi_j-\varphi_i) = \sum_i u_i\varphi_i^2 + t\sum_{\langle i,j\rangle}u_iu_j(\varphi_j-\varphi_i)^2\\ &= \underbrace{\sum_i\frac{\psi_i^2}{u_i}}_{\langle\psi|\widehat{1/u}|\psi\rangle} + t\sum_{\langle i,j\rangle}u_iu_j\left(\frac{\psi_j}{u_j}-\frac{\psi_i}{u_i}\right)^2 \geq \langle\psi|\widehat{1/u}|\psi\rangle.\end{aligned} \tag{1.30}$$

In the first equality of the second line we have used $\sum_i\sum_{j\in\partial i} = 2\sum_{\langle i,j\rangle}$. In the next equality we have rewritten one of the two copies of the sum over nearest-neighbors exchanging the indices i and j. The last inequality follows from the fact that all the components of $\mathbf{u}$ are non-negative, as stated in Eq. (1.24). Equation (1.30), is the same as Eq. (5) in [12], and represents the discrete version of Eq. (6) in [27].

The interpretation of $\widehat{1/u}$ as an effective potential implies that classically an electron with energy E can only occupy the set of sites i where $1/u_i < E$, i.e. where the effective potential energy is smaller than the energy of the electron. The main hypothesis of [12] is that, given this effective potential, this classical argument holds in general. Therefore, we can define the set of allowed sites as $\Omega_E = \{i|1/u_i \leq E\}$, and then study the statistical properties of the localization landscape to compute the

mobility edge as the critical curve for the percolation of the set Ω_E.

Chapter 2

Theoretical framework on the Bethe lattice

In this section we present the theoretical framework that we developed to study the localization landscape percolation problem on the Bethe lattice, and we summarize the well known solution of Anderson localization on the Bethe lattice. We start in Sec. 2.1 by deriving the cavity equations determining the fundamental physical quantities at stake, then (in Sec. 2.2)we present the localization landscape percolation problem and the equations that have to be solved to determine all its critical properties.

2.1 Cavity Analysis

In this section we derive the set of coupled equations that let us compute the localization landscape on a generic site i of the Bethe lattice as a function of independent cavity quantities defined on the subtrees rooted in the nearest neighbors of i. We present two different derivations, one based on the cavity method (used in a formulation implemented via Gaussian integrals which is explained in detail in Ref. [28]), which is completely self-contained, and another one which takes advantage of some known results for the Green's function of Anderson localization on the Bethe lattice. We start by presenting the self-contained derivation.

2.1.1 Derivation with auxiliary fields

The elements of the Green's function can be written as expectation values with a Gaussian measure as:

$$\mathcal{G}_{ij} = \mathbb{E}[x_i x_j] = \frac{1}{Z}\int \mathcal{D}x\, x_i x_j\, e^{-S_0[x]}\,, \tag{2.1}$$

where

$$S_0[x] = \frac{1}{2}\sum_i \varepsilon_i x_i^2 - t\sum_{\langle i,j\rangle} x_i x_j = \frac{1}{2}\mathbf{x}^{\mathbf{t}}\hat{\mathcal{H}}\mathbf{x} = \frac{1}{2}\mathbf{x}^{\mathbf{t}}\mathcal{G}^{-1}\mathbf{x}\,, \tag{2.2}$$

and

$$Z = \int \mathcal{D}x\, e^{-S_0[x]}. \tag{2.3}$$

This expression for the Green's functions is justified by the fact that, as we have written in Sec. 1.4, the Hamiltonian is positive definite, so $e^{-S_0[x]}/Z$ is a properly

normalized Gaussian measure. The integral defining the localization landscape follows from Eqs. (1.23) and (2.1), and reads

$$u_i = \frac{\int \mathcal{D}x\, x_i (\sum_j x_j)\, e^{-S_0[x]}}{Z}\,. \tag{2.4}$$

In order to compute this object, it is convenient to add a source term to the action that couples linearly to the field x:

$$S_J[x] = S_0[x] - J\sum_j x_j \qquad \Longrightarrow \qquad u_i = \left.\frac{\partial \mathbb{E}[x_i]}{\partial J}\right|_{J=0}\,. \tag{2.5}$$

In absence of the source term, all the variables x_i have zero mean, and their marginal distributions are just Gaussians centered in zero. In order to compute $\mathbb{E}[x_i]$ we need to find the cavity equations of the system in presence of the source term that breaks the parity of the marginal distribution. The most general form for the marginal distribution on a given site is

$$\mu_i(x_i) \propto e^{-\frac{x_i^2}{2\mathcal{G}_{ii}}+\xi_i x_i}\,. \tag{2.6}$$

This is a direct consequence of the Gaussian measure $e^{-S_0[x]}/Z$. Analogously, for the cavity lattice we can write the marginal on site i (root of the branch $B_{i\to j}$) as

$$\mu_{i\to j}(x_i) \propto e^{-\frac{x_i^2}{2\mathcal{G}_{i\to j}}+\xi_{i\to j} x_i}\,. \tag{2.7}$$

To find the recursion relations for the Green's function $\mathcal{G}_{ii}$ and the field ξ_i, we have to write the marginal on site i as the integral of the full measure $e^{-S_0[x]}/Z$ over all the variables $\{x_k\}_{k\neq i}$. Since the only variables coupled to x_i in $S_0[x]$ are the nearest neighbors $\{x_k\}_{k\in\partial i}$, the marginal on site i can be rewritten as an integral over $\{x_k\}_{k\in\partial i}$ of the terms in $e^{-S_0[x]}$ which depend on x_i, weighted with the joint probability distribution of $\{x_k\}_{k\in\partial i}$. Moreover, since $\{x_k\}_{k\in\partial i}$ are decoupled in $S_0[x]$, the joint probability distribution is separable as the product of the cavity marginals on each nearest neighbor in absence of i. The resulting equation is

$$\mu_i(x_i) = e^{-\frac{1}{2}\varepsilon_i x_i^2 + J x_i}\int \prod_{k\in\partial i}\left[\mathrm{d}x_k\, \mu_{k\to i}(x_k)\right] e^{t x_i \sum_{k\in\partial i} x_k} \propto e^{-\frac{1}{2}\varepsilon_i x_i^2 + J x_i + \frac{1}{2}\sum_{k\in\partial i}(\xi_{k\to i}+t x_i)^2 \mathcal{G}_{k\to i}}\,. \tag{2.8}$$

Analogously, for the marginal on site i in the cavity lattice we have

$$\mu_{i\to j}(x_i) = e^{-\frac{1}{2}\varepsilon_i x_i^2 + J x_i}\int \prod_{k\in\partial i\setminus j}\left[\mathrm{d}x_k\, \mu_{k\to i}(x_k)\right] e^{t x_i \sum_{k\in\partial i\setminus j} x_k} \propto e^{-\frac{1}{2}\varepsilon_i x_i^2 + J x_i + \frac{1}{2}\sum_{k\in\partial i\setminus j}(\xi_{k\to i}+t x_i)^2 \mathcal{G}_{k\to i}}\,. \tag{2.9}$$

Enforcing in Eqs. (2.8) and (2.9) the functional forms of Eqs. (2.6) and (2.7), one immediately obtains

$$\mathcal{G}_{ii}^{-1} = \varepsilon_i - t^2\sum_{k\in\partial i}\mathcal{G}_{k\to i}\,, \tag{2.10}$$

$$\xi_i = J + t\sum_{k\in\partial i}\mathcal{G}_{k\to i}\xi_{k\to i}\,, \tag{2.11}$$

$$\mathcal{G}_{i\to j}^{-1} = \varepsilon_i - t^2\sum_{k\in\partial i\setminus j}\mathcal{G}_{k\to i}\,, \tag{2.12}$$

$$\xi_{i\to j} = J + t\sum_{k\in\partial i\setminus j}\mathcal{G}_{k\to i}\xi_{k\to i}\,. \tag{2.13}$$

It is convenient to introduce the rescaled fields $\eta_{i\to j}$ such that $J\eta_{i\to j} = \xi_{i\to j}$, in terms of which the second and fourth equation read

$$\eta_i = 1 + t \sum_{k\in\partial i} \mathcal{G}_{k\to i}\eta_{k\to i}\,, \qquad \eta_{i\to j} = 1 + t \sum_{k\in\partial i\setminus j} \mathcal{G}_{k\to i}\eta_{k\to i}\,, \tag{2.14}$$

which is now completely independent of the value of the source J.

The last step is to express $\langle x_i\rangle$ in terms of the cavity fields. Since we know its marginal distribution (2.6) we just need to compute

$$\langle x_i\rangle = \int \mathrm{d}x_i\, x_i \mu_i(x_i) = \mathcal{G}_{ii} J\eta_i\,, \tag{2.15}$$

Finally, taking the derivative with respect to the source J, we get

$$u_i = \mathcal{G}_{ii}\eta_i\,. \tag{2.16}$$

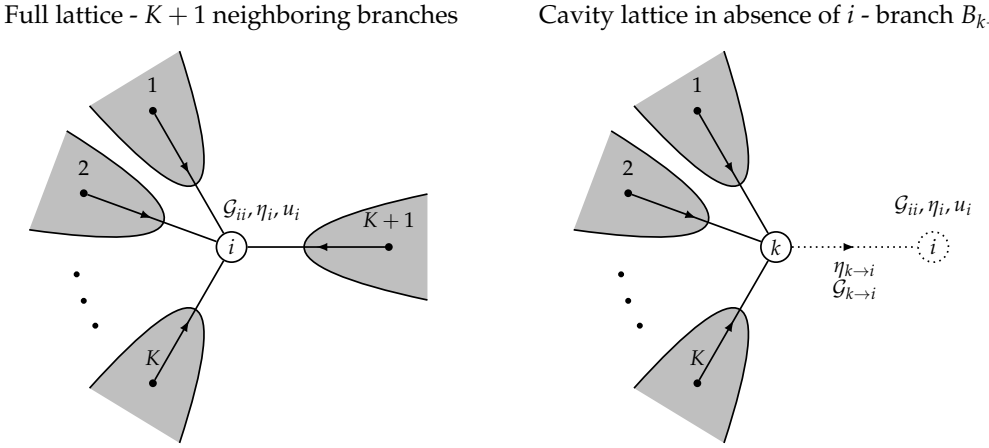

FIGURE 2.1: Left: Schematic representation of a Bethe lattice centered on a reference site i. $\mathcal{G}_{ii}$ and u_i, are the on-site quantities associated with this site. Right: The cavity subtree $B_{k\to i}$, rooted at a nearest neighbor $k \in \partial i$, obtained after removing site i from the lattice. The on-site quantities at i depend only on the cavity quantities $\{\mathcal{G}_{k\to i}, u_{k\to i}\}_{k\in\partial i}$, computed from the neighboring cavity subtrees $\{B_{k\to i}\}_{k\in\partial i}$.

2.1.2 Derivation with u alone

We can check that the previous result is correct by computing the u_i recursively using the standard cavity method on a tree (see Ref. [16]). Starting from Eq. (1.23) we have

$$u_i = \mathcal{G}_{ii} + \sum_{k\in\partial i} \sum_{j\in B_{k\to i}} \mathcal{G}_{ij}, \tag{2.17}$$

where $B_{k\to i} \equiv \{j \mid j \text{ belongs to the subtree rooted at } k \in \partial i \text{ after the removal of site } i\}$. The second sum can be written as:

$$\sum_{j\in B_{k\to i}} \mathcal{G}_{ij} = \mathcal{G}_{ik} + \sum_{j\in B_{k\to i}\setminus k} \mathcal{G}_{ij}. \tag{2.18}$$

We can write a Green's function $\mathcal{G}_{0r}$, where 0 and r are two sites on the Bethe lattice connected by a path of length r, using the following equations (whose derivation is

summarized in App. B):

$$\mathcal{G}_{0r} = \mathcal{G}_{00} \prod_{s=1}^{r} t\mathcal{G}_{s\to s-1} = \mathcal{G}_{rr} \prod_{s=0}^{r-1} t\mathcal{G}_{s\to s+1}. \tag{2.19}$$

Here the cavity Green's functions in the product are the ones connecting the sites along the path going from site r to site 0 (in the first equality) or vice versa (in the second). The recursive equations defining the normal and cavity Green's functions appearing in the formula are the ones of Eqs. (2.10) and (2.12), and their derivation analogous to the one in Sec. 2.1, with the only differences that we have to take $J = 0$ in the action (2.5), and $\xi_i, \xi_{i\to j} = 0$ in the ansatz for the normal and cavity measures (2.6) and (2.7).

Using Eq. (2.19) in Eq. (2.18), and after some algebra we obtain

$$u_i = \mathcal{G}_{ii} + t \sum_{k\in\partial i} \mathcal{G}_{i\to k} u_{k\to i}\,, \qquad u_{i\to j} = \mathcal{G}_{ii} + t \sum_{k\in\partial i\setminus j} \mathcal{G}_{i\to k} u_{k\to i}\,, \tag{2.20}$$

where we have defined

$$u_{k\to i} \equiv \sum_{j\in B_{k\to i}} \mathcal{G}_{kj}\,. \tag{2.21}$$

The detailed steps to obtain Eqs. (2.20) are given in App. C, where we also show that by defining

$$u_{i\to j} = \mathcal{G}_{ii}\eta_{i\to j}\,, \tag{2.22}$$

Eqs. (2.20) become equivalent to Eqs. (2.14).

As we can see, Eqs. (2.20) depend both on the normal and the cavity Green's functions, so Eqs. (2.10), (2.12), (2.20) represent a set of coupled recursive equations that can be solved self-consistently. Still, for the computation of the percolation critical curve it is more useful to work with the set of equations (2.10), (2.12) and (2.14) as it will be explained in the next section.

2.2 Localization landscape percolation equations

In this section we are going to derive the fundamental equation determining the critical behavior of our percolation problem. We start by deriving in Sec. 2.2.1 the cavity equation governing the probability that a generic site belongs to an infinite cluster, then in Sec. 2.2.2 we show how this equation and the cavity equations of Sec. 2.1 can be recast into a self-consistent distributional equation. Finally, in Sec. 2.2.3 we derive the expressions for the correlation function and the average cluster size.

2.2.1 Cavity analysis for the percolation probability

In order to study the percolation problem at energy E, one has to consider the standard cavity equation for the random site percolation on the Bethe lattice, where the probability of a node being occupied is replaced by the condition $u_i > 1/E$. In this setting we have to define

$$p_i \equiv \Pr\{\text{site } i \text{ belong to the giant cluster}\}. \tag{2.23}$$

These probabilities are the analogues of $p(q, q_B)$ in the site-bond percolation problem of Sec. 1.3, but now, since the value of the localization landscape on a site i is correlated to the ones of its nearest neighboring sites, the probability of a site being

occupied is site dependent. The recursive equations read

$$p_i = \theta(u_i > 1/E)\Big[1 - \prod_{k\in\partial i}(1 - p_{k\to i})\Big], \tag{2.24}$$

$$p_{i\to j} = \theta(u_i > 1/E)\Big[1 - \prod_{k\in\partial i\setminus j}(1 - p_{k\to i})\Big]. \tag{2.25}$$

From now on we will refer to the p_i's as the percolation probabilities. A fundamental observation is that $\{p_{k\to i}\}_{k\in\partial i\setminus j}$ in Eq. (2.24) are not statistically independent, because for each of them we need to compute the $\theta(u_k > 1/E)$'s, which depend also on quantities on site i. For this reason it is useful to switch to a different set of cavity variables that we define as

$$\begin{aligned}\bar{p}_{i\to j} &\equiv \Pr\{\text{cavity site } i \text{ (in absence of } j\text{) belong to the giant cluster if occupied}\}\\ &= \frac{p_{i\to j}}{\theta(u_k - 1/E)}\,.\end{aligned} \tag{2.26}$$

In terms of these variables Eqs. (2.24) become

$$p_i = \theta(u_i > 1/E)\Big[1 - \prod_{k\in\partial i}\Big(1 - \theta(u_k > 1/E)\bar{p}_{k\to i}\Big)\Big], \tag{2.27}$$

$$\bar{p}_{i\to j} = 1 - \prod_{k\in\partial i\setminus j}\Big(1 - \theta(u_k - 1/E)\bar{p}_{k\to i}\Big). \tag{2.28}$$

Since in the non-percolating phase all these probabilities must be exactly zero, close to the percolation critical curve we can linearize the second equation above, which becomes

$$\bar{p}_{i\to j} = \sum_{k\in\partial i/j}\theta(u_k - 1/E)\bar{p}_{k\to i}\,. \tag{2.29}$$

Here $u_k = \mathcal{G}_{kk}\eta_k$ (see Eq. (2.16)), and it can be computed in terms of independent cavity variables once we realize that

$$\mathcal{G}^{-1}_{kk} = \mathcal{G}^{-1}_{k\to i} - t^2\mathcal{G}_{i\to k}, \qquad \eta_k = \eta_{k\to i} + t\mathcal{G}_{i\to k}\eta_{i\to k}, \tag{2.30}$$

and

$$\mathcal{G}^{-1}_{i\to k} = \varepsilon_i - t^2\sum_{m\in\partial i\setminus k}\mathcal{G}_{m\to i}\,, \qquad \eta_{i\to k} = 1 + t\sum_{m\in\partial i\setminus k}\mathcal{G}_{m\to i}\eta_{m\to i}\,, \tag{2.31}$$

which follow from Eqs. (2.12). The final expression for the localization landscape for a site $k \in \partial i \setminus j$ is

$$\begin{aligned}u_k &= \left(\mathcal{G}^{-1}_{k\to i} - \frac{t^2}{\varepsilon_i - t^2\sum_{m\in\partial_k\setminus i}\mathcal{G}_{m\to i}}\right)^{-1}\left(\eta_{k\to i} + t\mathcal{G}_{k\to i}\frac{1 + t\sum_{m\in\partial_k\setminus i}\mathcal{G}_{m\to i}\eta_{m\to i}}{\varepsilon_i - t^2\sum_{m\in\partial_k\setminus i}\mathcal{G}_{m\to i}}\right)\\ &\equiv U_k(\{\mathcal{G}_{k\to i}, \eta_{k\to i}\}_{k\in\partial i}).\end{aligned} \tag{2.32}$$

2.2.2 Self-consistent distributional equation

We can now exploit the statistical independence of the cavity variables by observing that, after averaging over disorder, the Hamiltonian becomes translational invariant. Therefore, the joint probability distribution of on-site variables must be the same on every site (and the same must hold for the cavity variables). This means

that we can write a recursive equation that relates the joint probability distribution of $\mathcal{G}_{i\to j}, \eta_{i\to j}, \bar{p}_{i\to j}$ on a cavity site, to independent copies of itself. In other words, $\mathcal{G}_{i\to j}, \eta_{i\to j}, \bar{p}_{i\to j}$ are written in terms of independent sets of cavity variables $\{\mathcal{G}_{k\to i}, \eta_{k\to i}, \bar{p}_{k\to i}\}_{k\in\partial i}$ drawn from the same probability distribution $P(g,\eta,\bar{p})$. Because of translational invariance $P(g,\eta,\bar{p})$ must also be the probability distribution of $\mathcal{G}_{i\to j}, \eta_{i\to j}, \bar{p}_{i\to j}$ themselves. Therefore, using all the cavity equations defining the cavity variables, i.e. Eqs. (2.12), (2.14), (2.29) and (2.32), we can write the self-consistent distributional equation defining $P(g,\eta,\bar{p})$ as

$$P(g,\eta,\bar{p}) = \int d\varepsilon\, \gamma(\varepsilon) \left[\prod_{k=1}^{K+1} dg_k d\eta_k d\bar{p}_k\, P(g_k,\eta_k,\bar{p}_k)\right] \delta\left(g - \frac{1}{\varepsilon - t^2 \sum_{k=0}^{K} g_k}\right) \times \delta\left(\eta - 1 - t\sum_{k=1}^{K} g_k\eta_k\right) \delta\left(\bar{p} - \sum_{k=1}^{K} \theta\Big(U_k\big(\{g_k,\eta_k\}_{k\le K+1}\big) - 1/E\Big)\bar{p}_k\right). \tag{2.33}$$

Equation (2.33) can be solved using population dynamics, which is a standard numerical technique used to solve self-consistent distributional equations (it will be explained more in detail in App. D). This equation holds close to criticality. If one wants to obtain the distribution for a generic pair (E,W), the equation must be solved exchanging the delta function enforcing Eq. (2.29) with a delta enforcing the relation on the right in Eqs. (2.28).

Now, the critical curve of this percolation problem will be identified by the points in the (E,W)-plane where $\bar{p}_{i\to j}$ passes from having zero to non-zero expectation value. The comparison between the critical curve obtained with this method, and the one for Anderson localization will be done in Sec. 4.

2.2.3 Correlation function and average cluster size

From the definition in Eq. (1.16), considering all bonds as active, the correlation function becomes

$$C_p(r) = \Pr\{O_0 = 1, \dots, O_r = 1\} = \mathbb{E}\left[\prod_{i=0}^{r} O_i\right]. \tag{2.34}$$

Here the occupation variables O_i are the ones defined in Eq. (1.12), and the occupation condition is given by $u_i > 1/E$, thus

$$O_i = \begin{cases} 1 & \text{if } u_i > 1/E \\ 0 & \text{otherwise} \end{cases} \tag{2.35}$$

Now, since the correlation function can be written as an expectation value, and the random quantities in Eq. (2.34) depend only on the set of independent cavity quantities $\{(\mathcal{G}_{k\to i}, \eta_{k\to i}) \,|\, i \in \{0,\dots,r\}, k \in \partial\{0,\dots,r\}\}$, given the joint probability distribution $P(g,\eta,\bar{p})$ we can compute explicitly $C_p(r)$. The expected scaling of the correlation function for large distances is $C_p(r) \sim e^{-r/\xi_p}/K^r$. The procedure for the numerical computation of $C_p(r)$ and ξ_p is explained in App. E. After obtaining the correlation function, the average cluster size follows directly from Eq. (1.17), where $q = \Pr\{O_i = 1\}$ can be computed numerically from $P(g,\eta,\bar{p})$.

In Sec. 4 we present the results of the numerical computation of the percolation correlation length ξ_p and the inverse average cluster size $1/S$, comparing them with the Anderson correlation length ξ_{loc} and the IPR, that represent in some sense their counterparts in the Anderson Localization problem.

2.3 Anderson localization equations

In this section, we begin by summarizing the derivation of the equation that determines the Anderson localization transition on the Bethe lattice, whose numerical solution will be presented in Sec. 4. Then we give a sketch of the derivation of its related integral eigenvalue equation. This equation can be compared with Eq. (3.36), which represents its counterpart in the localization landscape percolation problem. This comparison will let us highlight the difference between the localization and the localization landscape percolation transitions on the Bethe lattice. The derivation presented in this section is a summary of the one in Ref.[18], with the only difference that now we consider the case with finite energy E.

2.3.1 Self-consistent distributional equation

For the Anderson localization solution, we work with the Hamiltonian with statistically symmetric spectrum, given in Eq. (1.1). For this system, it is well known that at the mobility edge, the local density of states ρ_i switches from being non-zero on $O(N)$ sites in the delocalized phase, to being exponentially small on $O(N)$ sites but $O(1)$ on $O(1)$ sites in the localized phase. As anticipated in Sec. 1.2, the local density of states is proportional to the imaginary part of $\mathcal{G}_{ii}(E - i0^+)$, where $\mathcal{G}_{ii}(z)$ is the Green's function defined by Eqs. (1.3) and (1.4). Therefore we can identify the mobility edge as the curve in the (E, W)-plane where the Green's functions transition from having zero to non-zero average imaginary part.

As in the percolation problem, we can work directly with the cavity quantities $\mathcal{G}_{i\to j}(z)$, taking $z = E - i\alpha$ where $\alpha \ll 1$ serves as a regularization parameter. From now on, to lighten the notation, we will write $\mathcal{G}_{i\to j}$ without explicit z-dependence. We decompose the cavity Green's function in the localized phase as

$$\mathcal{G}_{i\to j} = \mathcal{G}^R_{i\to j} + \mathrm{i}\alpha\mathcal{G}^I_{i\to j}. \tag{2.36}$$

Here, since in the localized phase $\mathrm{Im}[\mathcal{G}(E - i\alpha)]$ is linear in α for $\alpha \ll 1$, we have taken out a factor α from the imaginary part.

The cavity equation (1.9) can be separated into real and imaginary parts. By expanding for small α, and retaining the leading order, we obtain the two cavity equations governing the critical properties of the system:

$$(\mathcal{G}^R_{i\to j})^{-1} = E - \epsilon_i - t^2 \sum_{k\in\partial i\setminus j} \mathcal{G}^R_{k\to i}, \tag{2.37}$$

$$\mathcal{G}^I_{i\to j} = t^2(\mathcal{G}^R_{i\to j})^2 \sum_{k\in\partial i\setminus j} \mathcal{G}^I_{k\to i}. \tag{2.38}$$

As in the percolation case, these cavity equations can be recast into a distributional equation for the joint distribution $P(g, \hat{g})$ of $\mathcal{G}^R_{i\to j}$ and $\mathcal{G}^I_{i\to j}$, which reads

$$P(g,\hat{g}) = \int d\epsilon\, \gamma_s(\epsilon) \left[\prod_{k=1}^{K} dg_k d\hat{g}_k\, P(g_k,\hat{g}_k)\right] \delta\left(g - \frac{1}{E - \epsilon - t^2\sum_k g_k}\right) \delta\left(\hat{g} - t^2 g^2 \sum_k \hat{g}_k\right), \tag{2.39}$$

where the disorder distribution γ_s is the one in Eq. (1.2).

2.3.2 Solution through linear stability

Equation (2.39) can be rewritten as an integral eigenvalue equation using the following procedure.

Starting from Eq. (2.39), we use the integral representation of the delta function for the variable $\hat{g}$, which reads

$$\delta\left(\hat{g} - t^2 g^2 \sum_k g_k\right) = \int_{-\infty}^{\infty} \frac{d\lambda}{2\pi} e^{-i\lambda\left(g - t^2 g^2 \sum_k g_k\right)}, \tag{2.40}$$

to take the Fourier transform of the distributions on the right-hand side by integrating explicitly over all the g_k's. The result is

$$P(g,\hat{g}) = \int d\epsilon\, \gamma_s(\epsilon) \left[\prod_{k=1}^{K} dg_k d\hat{g}_k\, \hat{P}(g_k, \lambda t^2 g^2)\right] \delta\left(g - \frac{1}{E - \epsilon - t^2 \sum_k g_k}\right). \tag{2.41}$$

Then, Fourier transforming over $\hat{g}$ on both sides, we obtain

$$\hat{P}(g,\lambda) = \int d\epsilon\, \gamma_s(\epsilon) \left[\prod_{k=1}^{K} dg_k\, \hat{P}(g_k, \lambda t^2 g^2)\right] \delta\left(g - \frac{1}{E - \epsilon - t^2 \sum_k g_k}\right). \tag{2.42}$$

Next, we expand the characteristic function around the solution with zero imaginary part to lowest order in λ, assuming in the most general case a tail exponent β for the distribution:

$$\hat{P}(g,\lambda) \approx P(g) + f(g)|\lambda|^{\beta}, \tag{2.43}$$

which gives

$$f(g) = \int dg'\, \mathcal{K}^{\beta}_{loc}(g,g') f(g'). \tag{2.44}$$

Here, the kernel $\mathcal{K}^{\beta}_{loc}$ is

$$\mathcal{K}^{\beta}_{loc}(g,g') = K|tg|^{2\beta} \int d\epsilon d\tilde{g}\, \gamma_s(\epsilon) R_{loc}(\tilde{g}) \delta\left(g - \frac{1}{E - \epsilon - t^2(\tilde{g} + g')}\right), \tag{2.45}$$

where

$$R_{loc}(\tilde{g}) = \int \left[\prod_{k=1}^{K-1} dg_k\, P(g_k)\right] \delta\left(\sum_{k=1}^{K-1} g_k - \tilde{g}\right). \tag{2.46}$$

The function R_{loc} represent the distribution of the sum of $K-1$ real parts, and it can be evaluated numerically by computing the marginal distribution of the $\mathcal{G}^{R}_{i\to j}$'s through population dynamics (see App. D), and sampling from it sums of $K-1$ variables.

Given this equation, the critical curve will be identified by the curve in the (E,W)-plane where the top eigenvalue of the kernel is equal to one. In the localized phase, the only stable solution of the self-consistent distributional equation (2.39) must be the one with zero imaginary part of the Green's function, thus any perturbation $f(g)$ of this solution must vanish under iteration of the integral operator. On the other hand, in the delocalized phase the opposite must occur: any perturbation of the latter distribution must explode under iteration. If the top eigenvalue of $\mathcal{K}_{loc}$ is smaller than 1, decomposing the perturbation f on the eigenbasis of $\mathcal{K}_{loc}$, all components will vanish under iteration, conversely, if the top eigenvalue is greater than 1, all perturbations non-orthogonal to the eigenfunctions with eigenvalue greater than 1

will explode. Thus, the curve in parameter's space that separates these two regions is exactly the one where the maximum eigenvalue of the kernel is equal to one.

This integral operator can be diagonalized numerically with high precision, as it has been done in Refs. [29] and [30] for $E = 0$. Because of the high computational cost of this procedure, in order to obtain the full curve (sacrificing accuracy) we used the technique of Ref. [18]. This method will be explained in detail in App. E, and the resulting phase diagram will be presented in Sec. 4.

The integral eigenvalue equation (2.44) is fundamentally different from its counterpart in the localization landscape percolation problem. In Sec. 3.5.1, we will show this explicitly in the high-connectivity limit. This difference suggests that the critical behavior in Anderson localization may differ from the one of localization landscape percolation. A detailed comparison of their critical properties will be presented in Sec. 4.

Chapter 3

Results for percolation in the limit of high-connectivity

The high-connectivity limit represents the limit in which $K \gg 1$. In this regime many of the fundamental quantities describing the transition can be obtained either analytically, with few approximations, or with small numerical effort. Moreover, many of these results are very good approximations for low values of K (like the marginal distributions in Sec. 3.1 for the cavity Green's functions and the cavity localization landscapes), making the high-connectivity limit the perfect regime to study the main features of the transition without relying on numerical simulations.

The main idea behind the high-connectivity limit is that normal and cavity variables can be considered to be statistically equivalent, i.e.

$$\mathcal{G}_{ii} \overset{d}{=} \mathcal{G}_{i\to j}\,, \quad \eta_i \overset{d}{=} \eta_{i\to j}\,, \quad u_i \overset{d}{=} u_{i\to j} \overset{d}{=} \mathcal{G}_{i\to j}\eta_{i\to j}\,, \quad p_i \overset{d}{=} p_{i\to j} \;\; \forall i, \;\; \forall j \in \partial i\,, \tag{3.1}$$

where the symbol $\overset{d}{=}$ represents the equality in distribution. This is because recursive equations for normal and cavity variables differ by just one of the $O(K)$ terms inside sums of the type $\sum_{k\in\partial i}$ or $\sum_{k\in\partial i\setminus j}$, and according to large deviation theory, under the hypothesis that cavity variables are random variables with finite mean and variance, we can safely neglect one of the terms in the sums.

As we explained in Sec. 2.2 the sets of cavity variables $\{\mathcal{G}_{k\to i}, \eta_{k\to i}, p_{k\to i}\}_{k\in\partial i\setminus j}$ are not independent in the general case, because for each of the $p_{k\to i}$ one has to compute u_k, and all the u_k's are statistically dependent, since they depend on the quantities on their common neighbor i. Now, since $u_k \overset{d}{=} \mathcal{G}_{k\to i}\eta_{k\to i}$, the cavity percolation probabilities become independent cavity variables. For this reason, the three fundamental cavity equations that determine the transition in the high-connectivity limit are

$$\mathcal{G}^{-1}_{i\to j} = \varepsilon_i - t^2 \sum_{k\in\partial i\setminus j} \mathcal{G}_{k\to i}\,, \tag{3.2}$$

$$\eta_{i\to j} = 1 + t \sum_{k\in\partial i\setminus j} \mathcal{G}_{k\to i}\eta_{k\to i}\,, \tag{3.3}$$

$$p_{i\to j} = \theta(\mathcal{G}_{i\to j}\eta_{i\to j} > 1/E) \sum_{k\in\partial i\setminus j} p_{k\to i}\,, \tag{3.4}$$

where the last one have been obtained by expanding Eq. (2.25) for small cavity percolation probabilities close to the critical curve. The self-consistent distributional

equation that we have to solve is much simpler compared to Eq. (2.33), and reads

$$P(g,\eta,p) = \int d\varepsilon\, \gamma(\varepsilon) \int \left[\prod_{k=1}^{K} dg_k d\eta_k dp_k\, P(g_k,\eta_k,p_k)\right] \delta\left(g - \frac{1}{\varepsilon - t^2 \sum_k g_k}\right) \times \delta\left(\eta - 1 - t\sum_k g_k\eta_k\right)\delta\left(p - \theta(g\eta - 1/E)\sum_k p_k\right). \tag{3.5}$$

In Sec. 3.1 we will show that the marginal distributions of $\mathcal{G}_{i\to j}$, $\eta_{i\to j}$ and $u_{i\to j}$ admit thin-tailed solutions, and that these solutions are very close to the ones obtained with population dynamics simulations also for $K \sim O(1)$. In Sec. 3.2 we show numerically that the joint distribution $P(g,\eta)$ can effectively be approximated with the product of their marginals. In Sec. 3.3 we will derive a lower bound for the critical disorder. Next, in Sec. 3.4 we will compute the critical curve in the independent-site approximation, by considering the localization landscapes as independent random variables drawn from their marginal distribution. Finally, in Sec. 3.5 we present the derivations and numerical solutions of some of the equations determining the phase diagram in the high-connectivity limit.

3.1 Marginals

In order to obtain a self consistent solution for the marginal distribution of the cavity Green's function $P_g(g) = \int d\eta dp\, P(g,\eta,p)$, we observe that Eq. (2.12) is closed, therefore it can be solved independently from the other cavity equations. If K is big enough, assuming that P_g has finite mean and variance, in Eq. (2.12) we can approximate the sum over nearest neighbors of site i in absence of j as

$$\sum_{k\in\partial i\setminus j} \mathcal{G}_{k\to i} \approx K\mu_g + \sqrt{K\sigma_g^2}Y, \tag{3.6}$$

where

$$Y \sim \mathcal{N}(0,1), \quad \mu_g = \mathbb{E}[\mathcal{G}_{k\to i}], \quad \sigma_g^2 = \mathbb{V}[\mathcal{G}_{k\to i}]. \tag{3.7}$$

This follows directly from the central limit theorem. Now, the roughest approximation that we can make in Eq. (2.12) amounts to neglecting the gaussian fluctuations. In this limit the probability distribution of the cavity Green's functions is simply obtained by changing variables in the probability distribution of ε_i, i.e. the one of Eq. (1.21). Thus, the probability distribution of the cavity Green's functions in this approximation is

$$Q_g(g;\mu_g) = \begin{cases} \dfrac{1}{Wg^2} & \text{if } g \in D_g \equiv \left[\frac{1}{2t\sqrt{K}-t^2K\mu_g+W},\ \frac{1}{2t\sqrt{K}-t^2K\mu_g}\right] \\ 0 & \text{else.} \end{cases} \tag{3.8}$$

From this expression, μ_g and σ_g^2 are easily obtained self-consistently solving

$$\mu_g = \frac{1}{W}\ln\left|1 + \frac{W}{2t\sqrt{K} - t^2K\mu_g}\right|, \tag{3.9}$$

and computing

$$\sigma_g^2 = \frac{1}{(2t\sqrt{K} - t^2 K\mu_g)(2t\sqrt{K} - t^2 K\mu_g + W)} - \mu_g^2. \tag{3.10}$$

From numerical simulations with population dynamics we have observed that the distribution is quite accurate in mean and variance already for $K > 4$ and for all values of W. A more precise expression for the probability distribution of the cavity Green's functions can be found keeping the Gaussian fluctuations. Starting from

$$\mathcal{G}_{i\to j}^{-1} \approx \varepsilon - t^2\left(K\mu_g + \sqrt{K\sigma_g^2}Y\right), \tag{3.11}$$

we obtain

$$P_g(g;\mu_g,\sigma_g^2) = \frac{1}{Wg^2}\int_{2t\sqrt{K}}^{2t\sqrt{K}+W} d\varepsilon\, \mathcal{N}\left(\varepsilon\,; Kt^2\mu_g + 1/g\,,\, Kt^4\sigma_g^2\right), \tag{3.12}$$

where again mean and variance have to be obtained solving self-consistently the coupled equations

$$\mu_g = \int dg\, P_g(g\,;\mu_g,\sigma_g^2)g\,, \qquad \sigma_g^2 = \int dg\, P_g(g\,;\mu_g,\sigma_g^2)(g-\mu_g)^2\,. \tag{3.13}$$

We compute now the marginal distribution of the cavity rescaled fields by employing a similar approximation. We assume that

$$\eta_{i\to j} \approx 1 + t\left(K\mathbb{E}[\mathcal{G}_{k\to i}\eta_{k\to i}] + \sqrt{K\mathbb{V}[\mathcal{G}_{k\to i}\eta_{k\to i}]}Y\right), \quad \text{with } Y\sim\mathcal{N}(y\,;0,1)\,, \tag{3.14}$$

We will argue later that this gaussian approximation does not hold even in high-connectivity if the disorder is too high, but as we will see it is accurate enough to obtain a very good estimate of the marginal of the cavity localization landscapes also in low-connectivity. This is due to the fact that the distribution of the cavity Green's function is highly asymmetric in the strong disorder regime. For this reason, the asymmetry propagates to the distribution of the cavity rescaled fields, that loses its Gaussian shape.

In principle $\eta_{k\to i}$ and $\mathcal{G}_{k\to i}$ are not independent, therefore computing the expectation value and the variance of their product is not trivial. However, for high-connectivity, we can argue that they are weakly correlated. Therefore, we will use a mean-field approximation, considering them as independent, i.e.

$$P(g,\eta) = \int dp\, P(g,\eta,p) \approx P_g(g)P_\eta(\eta). \tag{3.15}$$

(this will be ckecked in the next section). This implies that the mean and variance in Eq. (3.14) now read

$$\mathbb{E}[\mathcal{G}_{k\to i}\eta_{k\to i}] = \mu_g\mu_\eta\,, \qquad \mathbb{V}[\mathcal{G}_{k\to i}\eta_{k\to i}] = \sigma_g^2\sigma_\eta^2 + \sigma_g^2\mu_\eta^2 + \sigma_\eta^2\mu_g^2\,. \tag{3.16}$$

where

$$\mu_\eta = \mathbb{E}[\eta_{k\to i}]\,, \qquad \sigma_\eta^2 = \mathbb{V}[\eta_{k\to i}]\,. \tag{3.17}$$

This implies that the probability distribution of the cavity rescaled fields is

$$P_\eta(\eta;\mu_\eta,\sigma_\eta^2) = \mathcal{N}(\eta\,;\mu_\eta,\sigma_\eta^2)\,, \tag{3.18}$$

with

$$\mu_\eta = \frac{1}{1 - Kt\mu_g}, \qquad \sigma_\eta^2 = \frac{Kt^2\sigma_g^2}{[1 - Kt^2(\sigma_g^2 + \mu_g^2)](1 - Kt\mu_g)^2}. \tag{3.19}$$

These expressions have been obtained by enforcing that both sides of Eqs. (3.14) have the same mean and variance.

The mean-field approximation in the derivation of P_η simplifies also the computation of the marginal distribution of the cavity localization landscapes, which follows directly from Eq. (3.15) and from the fact that now $u_{i\to j} \overset{d}{=} \mathcal{G}_{i\to j}\eta_{i\to j}$. The result is

$$\begin{aligned} P_u(u) &= \int dg\, P(g, \eta = u/g) \left|\frac{d(u/g)}{du}\right| = \int \frac{dg}{|g|} P_g(g) P_\eta(u/g) \\ &= \int dg\, P_g(g) \mathcal{N}(u; g\mu_\eta, g^2\sigma_\eta^2). \end{aligned} \tag{3.20}$$

We can observe that $u_{i\to j}$ is exactly the quantity whose mean and variance have

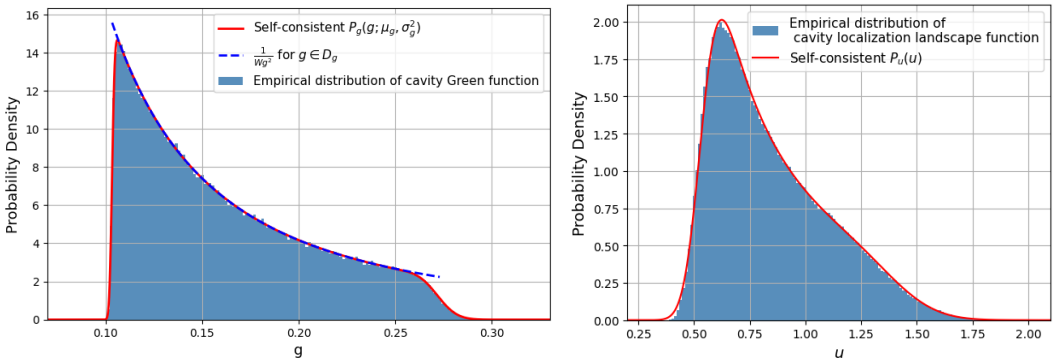

FIGURE 3.1: Marginal distributions of cavity Green's functions and cavity localization landscapes for $K = 5$, $t = 1$, and $W = 6$. Left: The probability distributions of $\mathcal{G}_{i\to j}$. Light blue histogram: empirical distribution of the cavity Green's functions obtained with population dynamics with $N = 5 \times 10^5$ sites. Red line: probability distribution in Eq. (3.12) with parameters μ_g and σ_g^2 computed solving by iteration the self consistent Eqs. (3.13). Blue line: rougher approximation for the probability distribution given in Eq. (3.8) with μ_g computed self-consistently iterating Eq. (3.9). Right: Probability distribution of $u_{i\to j}$. Light blue histogram: empirical distribution obtained using population dynamics for $N = 5 \times 10^5$ sites. Red line: probability distribution P_u in Eq. (3.20), with parameters μ_u and σ_u^2 obtained self-consistently from Eqs. (3.21).

been computed in Eqs. (3.16). Thus, using the results of equations (3.19) we have

$$\mu_u = \mu_\eta\mu_g = \frac{\mu_g}{1 - Kt\mu_g}, \qquad \sigma_u^2 = \frac{\sigma_\eta^2}{Kt^2} = \frac{\sigma_g^2}{[1 - Kt^2(\sigma_g^2 + \mu_g^2)](1 - Kt\mu_g)^2}. \tag{3.21}$$

In Fig. 3.1 we plotted the distribution $P_u(u)$, and the empirical distribution of $u_{i\to j} = \mathcal{G}_{i\to j}\eta_{i\to j}$ from population dynamics simulations.

3.2 Joint distribution $P(g,\eta)$

The joint probability distribution of the cavity Green's function and the cavity auxiliary fields $P(g,\eta)$ is the one satisfying the self-consistent distributional equation

$$P(g,\eta) = \int d\varepsilon\, \gamma(\varepsilon) \left[\prod_{k=1}^{K} dg_k d\eta_k\, P(g_k,\eta_k) \right] \delta\left(g - \frac{1}{\varepsilon - t^2 \sum_k g_k} \right) \delta\left(\eta - 1 - t \sum_k g_k \eta_k \right). \tag{3.22}$$

As we have anticipated in the previous section, we can check that $P(g,\eta)$ is well approximated by the product of the two marginals $P_g(g)$ and $P_\eta(\eta)$ as in Eq. (3.15) using numerics. The quality of the approximation can be quantified by computing the mutual information.

The mutual information of two continuous random variables X, Y distributed with P is defined as

$$I(X,Y) \equiv \int dxdy\, P(x,y) \log_2 \frac{P(x,y)}{P(x)P(x)}\,, \tag{3.23}$$

and it represents the information theoretical measure of the dependence of two random variables. More precisely, it is the information about the variable X that one obtains after measuring Y, quantified in terms of Shannon's entropy. The mutual information of two random variables is always greater or equal then zero. $I(X,Y) = 0$ corresponds to the case in which X and Y are statistically independent.

The estimation of the mutual information can be done using population dynamics (see App. D). Assuming that the population of N pairs of cavity Green's functions and cavity rescaled fields represents a set of N samples drawn from the exact distribution, we can compute $I(\mathcal{G}_{i\to j}, \eta_{i\to j})$ empirically through the procedure devised in Ref. [31] (we will not present explicitly the procedure in this work). We computed the mutual information with $K = 5$, $t = 1$ for many values of W in the range that will be used later to compute the critical curve. The results are plotted in Fig. 3.2. As we can see from the plot, the mutual information is of $O(10^{-2}\, bits)$ or less for the analyzed range of disorder, indicating that the mean-field approximation describes the real distribution with good accuracy for this set of parameters. Moreover, it has been checked that for a fixed value of the disorder, the mutual information decreases as K increases, signaling that the mean-field approximation improves increasing K.

In Fig. 3.3 we represented the colormap plots of the histograms of the joint probability distribution $P(g,\eta)$, and its mean-field approximation $P_g(g)P_\eta(\eta)$. The first one has been computed numerically through population dynamics, while the second one has been obtained by shuffling the g-variables between the pairs (g,η) in the latter distribution, erasing the dependencies of the two variables. As we can see from the plots the two distributions are qualitatively similar. The main difference between the two is that the tails of the distributions have a slightly different shape in the (g,η) plane. This is due to the fact that the values that $\eta_{i\to j}$ can take once $\mathcal{G}_{i\to j}$ is given are restricted by the coupled equations (3.2) and (3.3). As revealed from the mutual information measurements, this feature does not result in significant effects on the global dependency of the two variables. A result, as we have been able to check numerically for some points in the (E,W)-plane, is that the phase diagram computed using the population dynamics joint distribution, appears indistinguishable from the one obtained with the mean-field distribution. The phase diagrams obtained in the high-connectivity limit will be presented in Sec. 3.6.

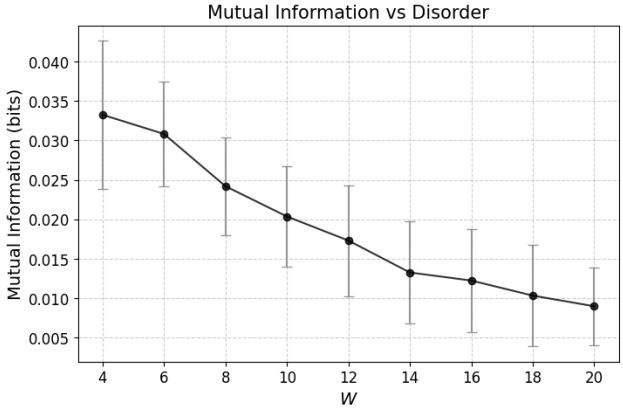

FIGURE 3.2: Mutual information of cavity Green's functions and cavity auxiliary fields. The mutual information, computed numerically following the procedure devised in Ref. [31], is plotted for many values of the disorder strength above the lower critical disorder W_c^{min} (see Sec. 3.3) for $K = 5$, $t = 1$. As it can be seen from the plot, the mutual information decreases monotonically with W, remaining always below $3.5 \cdot 10^{-2}\, bits$. This indicates that the mean-field approximation of Eq. (3.15) represents the exact joint distribution with good accuracy.

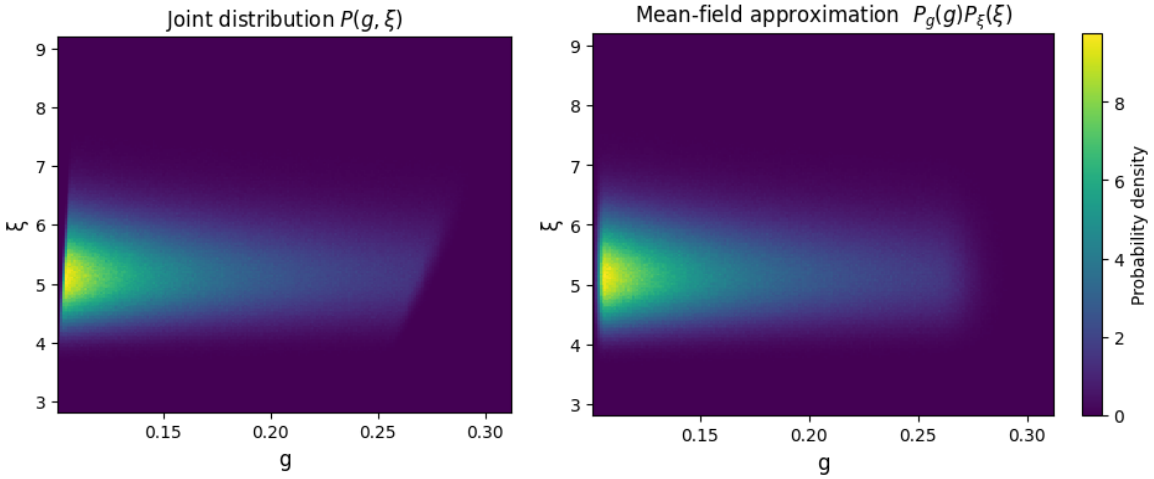

FIGURE 3.3: Plots of $P(g, \eta)$ and its mean-field approximation for $K = 5, t = 1$ and $W = 6$. Left: plot of the histogram of the joint probability distribution obtained through population dynamics (see App. D) with $N = 10^7$. Right: plot of the mean field approximation obtained by shuffling the cavity Green's functions of the pairs (g, η) in the histogram on the left. As it can be seen from the plot, the main qualitative differences are in the tails of the distribution, and they're due to the fact that for extreme values of $\mathcal{G}_{i\to j}$ the set of values that $\eta_{i\to j}$ can take are restricted by Eqs. (3.2),(3.3).

3.3 Lower bound for the critical disorder

It is important to observe that in order to be physically meaningful, the cavity rescaled fields must be non-negative (the opposite would imply that the localization landscapes are negative, which is impossible according to Eq. (1.24)). Thus, Eqs. (3.19) must be valid only in the regime where

$$\mu_\eta > 0 \iff \mu_g < \frac{1}{Kt}. \tag{3.24}$$

From Eq. (3.8) we can easily argue that μ_g is a decreasing function of the disorder. Moreover, for $W \to 0$, $\mu_g \to \frac{1}{t\sqrt{K}} > \frac{1}{Kt}$. Therefore, there must be a minimum value of the disorder W_c^{min} such that $\mu_g = \frac{1}{Kt}$, and below which the localization landscapes are not defined. As predicted, in numerical simulations we see that below this minimal disorder the recursion for the cavity rescaled fields has no fixed point, because the distribution of the $\eta_{i\to j}$'s keeps shifting to the right indefinitely, signaling that there is no solution with finite, positive, cavity rescaled fields. In this regime, the effective potentials $1/u_i$ are all equal to zero, which means that for any value of E the system will always be in the percolating (delocalized) phase. Using Eq. (3.9), we can approximate the value of the minimum critical disorder as the one solving the self consistent equation

$$W_c^{min} = Kt \ln \left| 1 + \frac{W_c^{min}}{t(2\sqrt{K} - 1)} \right| . \tag{3.25}$$

3.4 Critical curve in the independent-site approximation

The percolation problem can be solved in an approximate way by considering the u_i as independent. In this approximation we need to compute the probability that on a given site i the localization landscape u_i is greater than a fixed value $1/E$. This probability will be taken as the occupation probability of site i. Then, using the solution found in Sec. 1.3 for the uncorrelated percolation critical curve, we will be able to find the critical energy $E_c(W)$ for our system as the $E_c(W)$ such that at a given disorder W,

$$q_c \equiv \Pr\{u_i > 1/E_c(W)\} = 1/K. \tag{3.26}$$

The probability $\Pr\{u_i > 1/E\}$ can be computed in the high-connectivity limit using the assumption that $u_{i\to j}$ and u_i are statistically equivalent, i.e. that the latter probability can be computed using the marginal distribution of Eq. (3.20). Thus,

$$q = \Pr\{u_i > 1/E\} = \int du\, P_u(u)\theta(u - 1/E)\,. \tag{3.27}$$

The critical curve computed in this way has been plotted in Fig. 3.4 with a solid red line.

3.5 Exact critical curve in the high-connectivity limit

As anticipated at the beginning of section Sec. 3, in the following subsections we derive the equations that describe the critical curve in the high-connectivity limit in two different ways. The first one is based on defining an integral eigenvalue equation analogous to the one that we derived in Sec. 2.3.2. This derivation is important

to understand that the equations describing this percolation transition are fundamentally different from the ones describing the localization transition. The second method is more straight-forward, and it is based on enforcing that the average cluster size diverges at the transition.

3.5.1 Solution through linear stability

Following the same idea of [5], we start from the self-consistent distributional equation (2.33). Using the integral representation of the Dirac delta

$$\delta\left(p-\theta(g\eta-1/E)\sum_k p_k\right)=\int_{-\infty}^{\infty}\frac{d\lambda}{2\pi}\,e^{-\mathrm{i}\lambda\left(p-\theta(g\eta-1/E)\sum_k p_k\right)}\,, \tag{3.28}$$

we can rewrite

$$\begin{aligned}P(g,\eta,p)=\int\frac{d\lambda}{2\pi}\,e^{-\mathrm{i}\lambda p}\int d\varepsilon\,\gamma(\varepsilon)\int\left[\prod_{k=1}^{K}dg_k d\eta_k dp_k\,\hat{P}\left(g_k,\eta_k,\theta(g\eta-1/E)\lambda\right)\right]\\ \times\,\delta\left(g-\frac{1}{\varepsilon-t^2\sum_k g_k}\right)\delta\left(\eta-1-t\sum_k g_k\eta_k\right).\end{aligned} \tag{3.29}$$

Then, taking the Fourier transform of the latter we derive

$$\begin{aligned}\hat{P}(g,\eta,\lambda)=\int d\varepsilon\,\gamma(\varepsilon)\int\left[\prod_{k=1}^{K}dg_k d\eta_k\,\hat{P}\left(g_k,\eta_k,\theta(g\eta-1/E)\lambda\right)\right]\\ \times\,\delta\left(g-\frac{1}{\varepsilon-t^2\sum_k g_k}\right)\delta\left(\eta-1-t\sum_k g_k\eta_k\right).\end{aligned} \tag{3.30}$$

The theta function in the argument of the characteristic function of the distribution distinguishes between two cases. For $g\eta > 1/E$ we have to solve the integral equation

$$\hat{P}(g,\eta,\lambda)=\int d\varepsilon\,\gamma(\varepsilon)\int\left[\prod_{k=1}^{K}dg_k d\eta_k\,\hat{P}\left(g_k,\eta_k,\lambda\right)\right]\delta\left(g-\frac{1}{\varepsilon-t^2\sum_k g_k}\right)\delta\left(\eta-1-t\sum_k g_k\eta_k\right), \tag{3.31}$$

while for $g\eta < 1/E$ we simply have

$$\hat{P}\left(g_k,\eta_k,\theta(g\eta-1/E)\lambda\right)=\hat{P}\left(g_k,\eta_k,0\right)=P\left(g_k,\eta_k\right), \tag{3.32}$$

thus

$$P(g,\eta,p)=P(g,\eta)\delta(p), \tag{3.33}$$

In order to find an equation for the critical curve, we are interested in finding a solution for the probability distribution that admits a finite expectation value of the cavity percolation probability. Since its distribution necessarily has finite mean and variance (because $p\in[0,1]$), we can assume that at criticality the characteristic function for $g\eta > 1/E$ can be expanded in powers of λ, and that the term of the smallest order is exactly of order one:

$$\hat{P}(g,\eta,\lambda)=P(g,\eta)+i\lambda f(g,\eta)+O(\lambda^2). \tag{3.34}$$

Substituting in the integral Eq. (3.31), and discarding terms of order higher than one we obtain a self consistent equation for $f(g,\eta)$ that reads

$$f(g,\eta) = K\int d\varepsilon\,\gamma(\varepsilon)\,dg'd\eta'\,f(g',\eta')\left[\prod_{k=1}^{K-1} d\eta_k dg_k\,P(g_k,\eta_k)\right] \times \delta\left(g-\frac{1}{\varepsilon-t^2\left(g'+\sum_{k=1}^{K-1}g_k\right)}\right)\delta\left(\eta-1-t\left(g'\eta'+\sum_{k=1}^{K-1}g_k\eta_k\right)\right), \tag{3.35}$$

and can be recast as

$$f(g,\eta) = \int dg'd\eta'\,\mathcal{K}_p(g,\eta,g',\eta')f(g',\eta'), \tag{3.36}$$

with

$$\mathcal{K}_p(g,\eta;g',\eta') = \int d\varepsilon d\tilde{g}d\tilde{u}\,\gamma(\varepsilon)R_p(\tilde{g},\tilde{u})\delta\left(g-\frac{1}{\varepsilon-t^2(g'+\tilde{g})}\right)\delta\left(\eta-1-t\left(g'\eta'+\tilde{u}\right)\right), \tag{3.37}$$

where we have introduced the joint probability distribution of the sums $\sum_{k=1}^{K-1} g_k$ and $\sum_{k=1}^{K-1} g_k\eta_k$:

$$R_p(\tilde{g},\tilde{u}) \equiv \int\left[\prod_{k=1}^{K-1} dg_k d\eta_k\,P(g_k,\eta_k)\right]\delta\left(\sum_{k=1}^{K-1}g_k-\tilde{g}\right)\delta\left(\sum_{k=1}^{K-1}g_k\eta_k-\tilde{u}\right). \tag{3.38}$$

Performing the integrals over the tilde variables, the kernel simplifies to

$$\mathcal{K}_p(g,\eta;\,g',\eta') = \frac{K}{g^2\,t^3}\int d\varepsilon\,\gamma(\varepsilon)R_p\left(-g'-\frac{1-\varepsilon g}{gt^2},\;-g'\eta'-\frac{1-\eta}{t}\right). \tag{3.39}$$

Now, in the non-percolating phase, the solution with zero percolation probability, i.e. $P(g,\eta,p) = P(g,\eta)\delta(p)$, is the stable one. This means that any infinitesimal perturbation of its characteristic function, under iteration of the recursive equation defining $\hat{P}(g,\eta,\lambda)$ will vanish. Instead, in the percolating phase, we expect that the first-order perturbative term will increase under iteration. Accordingly, the critical curve will be identified as the curve in the space of parameters where the first order correction remains stable under iteration, i.e. where the kernel $\mathcal{K}_p$ has top eigenvalue equal to 1 (following exactly the same argument at the end of Sec. 2.3.2). The integral operator can be computed numerically, using population dynamics to evaluate the distribution $R_p(\tilde{g},\tilde{u})$, and it can be diagonalized numerically to obtain the critical curve with very high precision. This method is highly computationally expensive, therefore in order to compute the critical curve in the high-connectivity limit we used a completely different technique that we present in the next section.

3.5.2 Solution through the divergence of the average cluster size

An alternative method to determine the critical curve involves deriving an expression for the average cluster size S and identifying the values (E,W) for which S diverges.

In the general case, a cluster consists of a connected component of lattice sites i where $u_i > 1/E$. The statistical dependence between u_i and u_k (for $k \in \partial i$) is complex, but in the high-connectivity limit the problem simplifies significantly. Here, we can treat $u_k \overset{d}{=} u_{k\to i} \overset{d}{=} \mathcal{G}_{k\to i}\eta_{k\to i}$, effectively breaking the mutual dependence

between sites i and k: u_i depends on all its neighbors, while $u_{k\to i}$ depends on all its neighbors except i.

In this high-connectivity limit, we can replace the occupation variable O_i from Eq. (2.35) with

$$O_{i\to j} = \begin{cases} 1 & \text{if } u_{i\to j} > 1/E \\ 0 & \text{otherwise} \end{cases} . \tag{3.40}$$

By substituting in the definition of Eq. (2.34) the set of occupation variables $\{O_1, \ldots, O_r\}$ with $\{O_{1\to 0}, \ldots, O_{r\to r-1}\}$, we can factorize Eq. (2.34) as

$$\begin{aligned} C_p(r) &= \Pr\{O_0 = 1, O_{1\to 0} = 1, \ldots, O_{r\to r-1} = 1\} \\ &= \left[\prod_{s=2}^{r} \Pr\{O_{s\to s-1} = 1 \mid O_{s-1\to s-2} = 1\}\right] \Pr\{O_{1\to 0} = 1 \mid O_0 = 1\} \Pr\{O_0 = 1\} . \end{aligned} \tag{3.41}$$

Due to translational invariance, the conditional probability that a site is occupied given that one of its nearest neighbors is occupied is independent of the specific pair of sites. Thus, we define

$$\bar{q} \equiv \Pr\{O_{k\to i} = 1 \mid O_{i\to j} = 1\} \quad \forall i, \forall j \in \partial i, \forall k \in \partial i \setminus j . \tag{3.42}$$

Similarly, the last factor of Eq. (3.41) is given by the unconditional occupation probability $q \equiv \Pr\{O_i = 1\}$. Using these definitions, $C_p(r)$ takes the form

$$C_p(r) = q\bar{q}^r = \frac{q}{K^r} e^{-r/\xi_p}, \tag{3.43}$$

where the correlation length is given by

$$\xi_p = -\frac{1}{\ln K\bar{q}}. \tag{3.44}$$

As in the independent-site percolation problem (Sec. 1.3), the correlation function decays exponentially, so the average cluster size, defined in Eq. (1.17), simplifies to

$$S = \frac{1+\bar{q}}{1-K\bar{q}}. \tag{3.45}$$

We immediately see that S diverges when

$$\bar{q} = \bar{q}_c = 1/K. \tag{3.46}$$

This condition is analogous to that of the independent percolation problem, except that the occupation probability is now conditioned on the occupation of a neighboring site. By numerically evaluating the pairs (E, W) that satisfy $\bar{q} = 1/K$, we obtain the critical curve. The numerical procedure to compute $\bar{q}$ is explained in detail in App. E.

3.6 Results for the phase diagrams

Figure 3.4 presents the two phase diagrams obtained in the high connectivity limit using both the independent-site approximation condition (Eq. 3.26), and the exact condition (Eq. 3.46). It should be noted that the correct computation of the exact

curve for a given parameter pair (K, t) requires sampling from the joint distribution $P(g, \eta)$, as this properly accounts for correlations between cavity Green's functions and rescaled fields. However, we have observed numerically in Sec. 3.2 that the mean-field approximation of Eq. (3.15) describes with good accuracy the joint distribution $P(g, \eta)$. For this reason, the exact curve was computed by sampling from the self-consistent marginal distributions derived in Sec. 3.1, reducing significantly the computational time. As anticipated in Sec. 3.2, we have checked that the curve obtained this way shows an excellent agreement with the points obtained using the joint distribution computed via population dynamics. The numerical procedures employed are described in detail in App. E.

Another remark is that, even though the high-connectivity equations are correct only for $K \gg 1$, many of the probability distributions of Sec. 3.1 are accurate already for $K = 5$, for example the marginals of the cavity localization landscapes and the cavity Green's functions (see Fig. 3.1). For this reason, we plot the two curves for $K = 5$ (solid black line in Fig. 3.4), arguing that the one obtained with the exact high-connectivity condition properly describes many important features of the real curve for $K = 5$, even though we are neglecting the influence of one neighbor out of six. Moreover, the Bethe lattice with $K = 5$ represent the Bethe approximation of the solution for the cubic lattice, allowing direct comparison of our phase diagram with the one obtained numerically in Ref. [12].

The first observation for the phase diagrams is that the independent-site curve deviates significantly from the exact one, this indicates that the correlations between nearest neighboring sites are fundamental to describe the physics of the system, and neglecting them leads to wrong results.

Next, comparing the image on the right in Fig. 3.4 with the phase diagram computed by Filoche in Ref. [12], we see that the results are qualitatively similar, with the only difference that on the Bethe lattice the spectral boundary prevents the curve from reaching zero disorder (see Sec. 3.3). The plot on the right has been obtained from the black curve in the left image by translating the energies of a quantity $-2t\sqrt{K} - W/2$, in order to get back to the Hamiltonian with statistically symmetric spectrum, and sending $E \to -E$ (employing this symmetry) to visualize only the positive-energy part of the phase diagram (which is symmetric with respect to the W axis). For this reason, in the right image the percolating and non-percolating phases are exchanged. It is interesting to notice that the lower bound for the critical disorder derived in Sec. 3.3, predicts with high accuracy the value of the disorder where the critical curves cease to exist.

Now, what we aim to do is to understand if the localization landscape percolation on the Bethe lattice is able to describe the Anderson transition. To do so, the high-connectivity solution is not enough, in fact the computational time needed to obtain the mobility edge for Anderson localization is very high for high K, therefore it is much faster to compute both the Anderson and percolation critical curves for $K = 2$. Therefore, for the percolation transition we need to use the general equations given in Sec. 2.2, exact for any value of the connectivity.

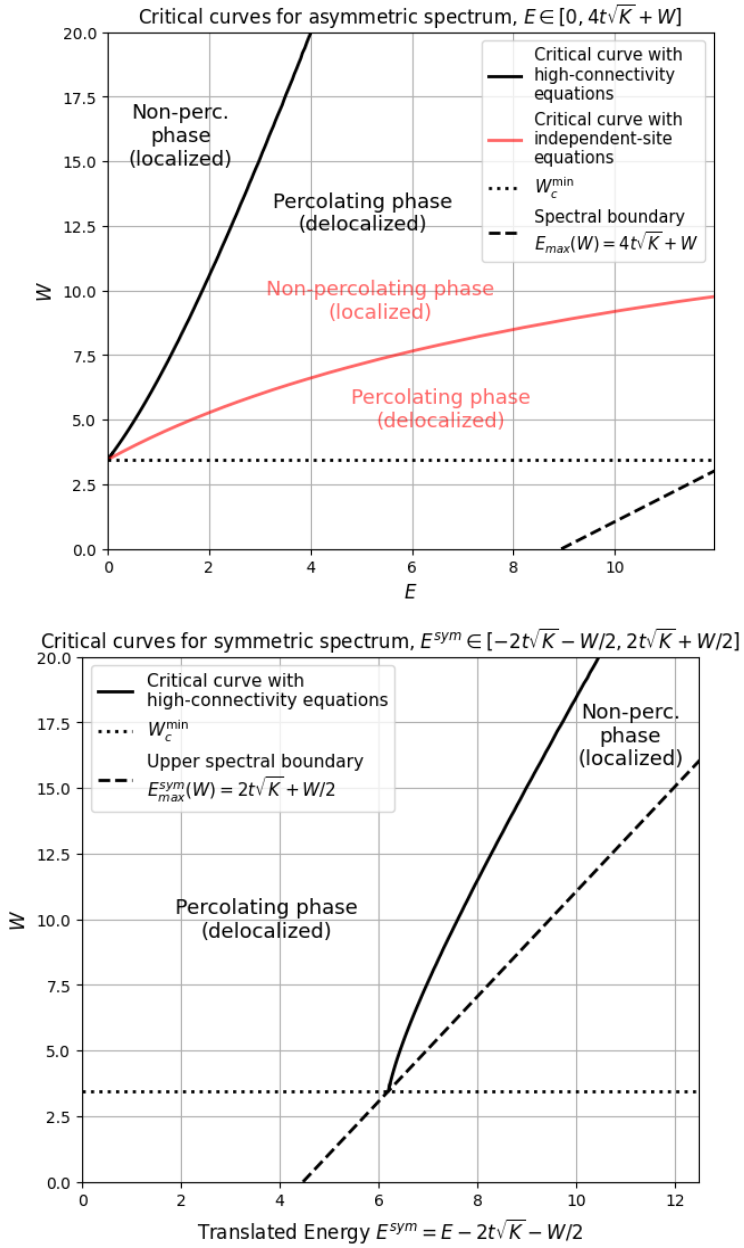

FIGURE 3.4: Percolation phase diagrams for $K = 5$ and $t = 1$. Top: positive definite Hamiltonian defined at the beginning of Sec. 1.4. Red curve: critical curve separating percolating and non-percolating phases for high-connectivity in the independent-site approximation (Eq. 3.26). Black line: exact critical curve in the high-connectivity limit (Eq. 3.46). Dashed line: upper bound of the spectrum, i.e. $E_{max}(W) = 4t\sqrt{K} + W$ (see Sec. 1.4). Dotted line: analytically predicted lower critical disorder (Eq. 1.26). Bottom: Hamiltonian with the statistically symmetric spectrum of (Eq. 1.1). Black curve: high-connectivity curve obtained from the black curve of the top image as described in Sec. 3.6.

Chapter 4

Comparison of the transitions

In this section we compare the results for the critical properties of Anderson localization computed through the numerical solution of Eq. (2.39), and the ones obtained with Eq. (2.33) introduced in Sec. 2.2 for the percolation problem.

4.1 IPR vs $1/S$

As mentioned in Sec. 1.2, the IPR is a measure of the inverse volume occupied by an eigenfunction, for this reason its natural counterpart in the localization landscape percolation problem is the inverse of the average cluster size $1/S$. Both of them can be computed numerically sampling from the joint probability distributions $P(g, \hat{g})$ and $P(g, \eta) = \int d\bar{p}\, P(g, \eta, \bar{p})$ respectively. $P(g, \hat{g})$ is the one satisfying Eq. (2.39). The detailed numerical procedure, optimized for the computation of Anderson localization IPR and C_{loc}, is the one explained in Ref. [18], which actually uses the distribution $P(\mathrm{Re}[1/\mathcal{G}_{ii}],\ \mathrm{Im}[1/\mathcal{G}_{ii}])$, but it will not be described in this text. $P(g, \eta, \bar{p})$ is the one in Eq. (2.33), where after integrating over $\bar{p}$, the delta function relative to $\bar{p}$ disappears, resulting again in the expression of Eq. (3.22). The detailed procedure for the numerical computations are devised in App. E.

As we can see in the plot on the left of Fig. 4.1, the IPR and the inverse average cluster size $1/S$ have completely different behaviors, one jumps from zero to a finite value at criticality, while the other grows linearly from zero. The critical behavior of the IPR on the Bethe lattice has not been completely understood. Even though it is well known that it jumps at the transition, the critical exponent has not been established yet. In the plot we fitted the six points closest to the transition to a square root law (following the conjecture of Ref. [18]), obtaining a good agreement very close to criticality. However, the error bars (that we have not plotted) are large, therefore we cannot state anything about the critical exponent of the IPR. The inverse average cluster size appears to follow a linear growth starting from zero at criticality. The critical exponent of $1/S$ for the standard site-percolation on the Bethe lattice is known exactly, and is $\gamma = 1$. This behavior is apparently well satisfied also further from criticality by the localization landscape percolation datapoints. Here, the error bars are much smaller than the ones of the IPR, thus we can say with higher confidence that the $1/S$ in the localization landscape percolation problem has the same critical exponent as the standard site percolation.

4.2 Correlation lengths

The correlation functions for Anderson localization and the localization landscape percolation problem, defined in Sec. 1 in Eqs. (1.16) and (1.7) respectively, can be compared close to criticality by computing numerically their respective correlation

lengths ξ_{loc} and ξ_p. The two correlation lengths are computed by fitting the functional form of their asymptotic behavior (i.e. $C(r) \sim e^{-r/\xi}/K^r$ for $r \gg 1$) to the correlations functions computed numerically. The computation for the Anderson localization correlation function have been done following the procedure in Ref. [18], while for the percolation correlation function the numerical methods are explained in detail in App. E. As we see from the plot on the right of Fig. 4.1, both the correlation lengths diverge at criticality with the same power law (as we expect, since the critical exponent of the correlation length is $\nu = 1$ for both Anderson localization and site percolation on the Bethe lattice) but with a different prefactor, indicating that the two quantities are not equivalent. The error bars for Anderson data are again much bigger than the ones of localization landscape percolation. As it is evident from the plot on the right, the agreement of the Anderson data with the expected critical behavior is slightly worse, but this is most likely due to the lower accuracy of the measurements.

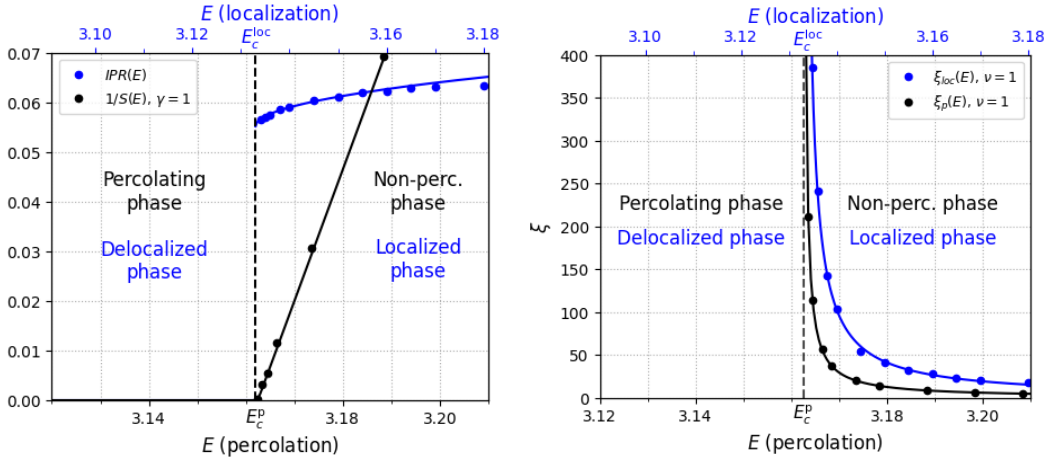

FIGURE 4.1: Critical behaviors of the IPR, $1/S$, ξ_{loc} and ξ_p. The datapoints have been computed numerically around the critical energy for parameters $W = 1.5$, $K = 2$, $t = 1$. $W = 1.5$ is one of the disorder values where the critical energies of the two problems are the closest. The Anderson and percolation results are plotted w.r.t. two different x-axes, which differ only by a translation that makes the two critical energies match. The Anderson points and curves (in blue) are related to the blue x-axis on top of the plots, while the percolation points and curves (in black) follow the black x-axis on bottom. Left: IPR and $1/S$ vs E. It is well known that the IPR on the Bethe lattice jumps from zero to a finite value at the transition. The first six points immediately on the left of the Anderson localization transition has been fitted to a square root law, following the conjecture for the critical behavior of the IPR in Ref. [18]. The inverse average cluster size $1/S$ has been fitted to a line, since the critical exponent of $1/S$ for site percolation on the Bethe lattice is $\nu = 1$. Right: ξ_{loc} and ξ_p vs E. Both the correlation length of Anderson and the one of localization landscape percolation appear to diverge with critical exponent $\nu = 1$. This is in agreement with the known results for Anderson localization and site percolation on the Bethe lattice.

4.3 Transitions

In Fig. 4.2 we plot the critical curves of the Anderson localization (blue line) and localization landscape percolation (black line) problems. The transition curves have been obtained with similar numerical procedures. For Anderson localization, as

anticipated in Sec. 2.3.1, we searched for the values of (E, W) where that the expectation value of the imaginary part of the Green's function for the statistically symmetric Hamiltonian of Eq. 1.1 passes from being zero (in the localized phase) to non-zero (in the delocalized phase). To do this, we followed the procedure devised in Ref. [18] to compute the expectation value of the imaginary part of the Green's function for many values of E (fixing the disorder W), searching for the critical energy where this becomes non-zero. For the localization landscape percolation instead, fixing the value of the disorder W, we computed the joint probability distribution $P(g, \eta, \bar{p})$ that satisfies Eq. (2.33) via population dynamics for many values of E in the non-percolating phase, searching for the critical energy $E_c(W)$ where $\int dg d\eta d\bar{p}\, P(g, \eta, \bar{p})\hat{p}$ becomes non zero, and averaging over many realizations of the measurement. The two critical curves are very different as it is evident from the plot. This indicates that for the Bethe lattice the localization landscape framework cannot predict the position of the mobility edge. This is a very important result, because it shows that despite the apparently good results of localization landscape percolation on the cubic lattice, obtained numerically by Filoche in [12], this proposal fails to accurately predict the mobility edge's position on arbitrary lattices. It is interesting to notice that the lower critical disorder for the percolation transition, derived in the high-connectivity limit, predicts with very high accuracy the position where the percolation critical curve touches the spectral boundary, ceasing to exist.

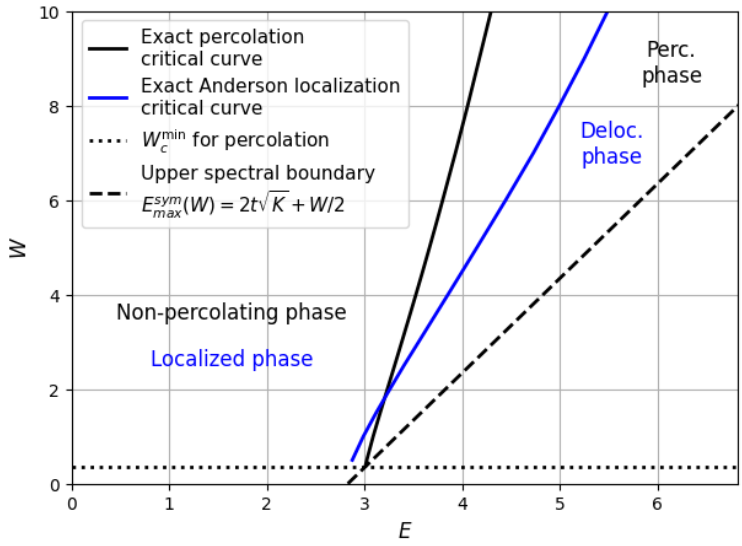

FIGURE 4.2: Phase diagram of the Anderson model for $K + 1 = 3$ in the (E, W) plane (positive energy region). The spectrum is statistically symmetric, therefore there is a symmetric phase diagram for negative energies. Black dashed line: upper bound of the spectrum, defined by $E_{\text{max}}^{\text{sym}} = 2t\sqrt{K} + W/2$ (as mentioned in Sec. 1.4). Blue line: mobility edge marking the critical curve for Anderson localization on the Bethe lattice, obtained by identifying the (E, W) values where the imaginary part of the Green's function transitions from zero to finite expectation value. Green dots: percolation critical curve obtained, searching for the curve where $\mathbb{E}[\bar{p}_{i\to j}]$ transitions from being zero to non-zero. Black dotted line: lower bound for the critical disorder predicted by the high-connectivity limit solution (see Sec. 3.3).

4.4 Discussion

According to inequality (1.26), the localization landscape should represent an upper bound to the amplitude of the eigenfunctions. For this reason, one expects that the critical energy predicted by the localization landscape framework should be an upper bound for $E_c(W)$ of Anderson localization, and this is exactly what has been observed numerically on the cubic lattice by Filoche in [12]. What we found instead is that the localization landscape percolation and Anderson localization critical curves cross, indicating that the Anderson localized phase is not a subregion of the percolating phase for the Bethe lattice.

We believe that the result of Filoche should not be expected in general when using the localization landscape percolation approach to obtain the critical curve. In Ref. [12], it is argued that the inverse localization landscape has the interpretation of an effective potential, and this is the property that motivates the choice of using a percolation approach with the occupation condition given by $1/u_i < E$. According to this effective potential interpretation, one would expect that the region in the phase diagram where the effective potential basins percolate through the lattice could be interpreted as the part of the Anderson localization phase diagram where delocalization can be described classically, and that the delocalized phase would extend further once quantum tunneling of electrons through effective potential barriers is allowed. This means that, if one defines the percolation in this way, the expected outcome should be the opposite of the one described in the previous paragraph.

We believe that this contradiction derives from employing the effective potential interpretation to define the percolation problem. The reason for the failure of localization landscape percolation in describing the upper bound to $E_c(W)$ of Anderson localization on a generic lattice could be the fact that the inverse localization landscape is the potential of a Schrödinger equation for the function $\varphi(\mathbf{x})$ (Eq. 1.29), not for the electronic wavefunctions, and this could cause it to lose its property of classically confining the electrons.

This can be understood by looking at the fundamental inequality of "Localization Landscape Theory", i.e., Eq. (1.26). Since the maximum value of its l.h.s. is 1, we realize that the condition $1/u_i < E$, which we used for percolation, actually indicates whether the maximum of an eigenfunction can be at site i or not. This means that in the percolation approach we have considered as unoccupied all the sites where an eigenstate cannot be at its maximum, not those that are classically allowed.

If one wanted to compute the true classically allowed regions, the exact potential to be used would have been the disordered potential ϵ_i of Anderson localization, but since localization is a strongly quantum phenomenon, the bound produced by the occupation condition $\epsilon_i < E$ is not useful for describing the phase diagram.

In conclusion, we think that the main flaw in this approach is in the mapping of the exact result of Eq. (1.26) in the localization landscape percolation problem that we have studied. Thus, even though the localization landscape percolation approach seems to work on a Euclidean lattice, in order to actually describe the upper bound defined by "Localization Landscape Theory" on a generic lattice, one should define a more rigorous criterion employing directly inequality (1.26).

Conclusion

In this work we performed a detailed comparison between the critical behavior predicted by the percolation problem defined using "Localization Landscape Theory" and the exact results for Anderson localization on the Bethe lattice. While the localization landscape framework provides an appealing physical picture, in which the delocalization transition is interpreted as a percolation of classically allowed regions, we have shown that this analogy fails to reproduce the true critical properties of the Anderson transition for the Bethe lattice. This indicates that, despite the apparently good results observed numerically on the cubic lattice [12], the framework is not suited to describe the Anderson localization phenomenon on a generic lattice.

Specifically, we derived the self-consistent equations governing the percolation probability of the set $\Omega_E = \{i \,|\, 1/u_i \leq E\}$ on the Bethe lattice, and solved them both analytically in the high-connectivity limit and numerically through population dynamics in the general case. The resulting critical curve $E_c(W)$, obtained from the percolation of the landscape valleys, does not match the known mobility edge derived from the Anderson localization exact solution on the Bethe lattice. Moreover, the comparison between the correlation length ξ_p and average cluster size S in the localization landscape framework, and their Anderson counterparts ξ_{loc} and IPR, show significant discrepancies in scaling behavior near criticality. We believe that the discrepancy derives from the intrinsic differences in the nature of the two transitions. Anderson localization is governed by quantum interference and the behavior of the imaginary part of the Green's function, while the localization landscape percolation transition is not only entirely classical, but also obtained through an approximate interpretation of the inverse localization landscape as an effective potential for electrons.

Although the "effective potential" captures regions of localization, the statistical percolation properties of the regions where $1/u_i > E$ are not sufficient to reproduce the critical curve and universality class of the Anderson transition. Moreover, contrarily to what it was believed, it cannot even provide an upper bound to Anderson localization's critical energies $E_c(W)$, since the two critical curves cross.

A posteriori, we believe that this percolation problem is not able to effectively make use of the fundamental inequality of "Localization Landscape Theory" (Eq. 1.26), since the effective potential percolation problem is defined employing the approximate interpretation of $1/u_i$ as an effective potential. However, that with a more rigorous approach, it could be possible to define from "Localization Landscape Theory" a percolation problem whose solution could represent an actual upper bound to the Anderson localization critical energies on a generic lattice.

Finally, we conclude that the localization landscape percolation framework should be used with caution while studying localization on finite-dimensional systems. However, this does not disqualify "Localization Landscape Theory" as a proposal that has the potential to be able to derive important results for the understanding of Anderson transition, if applied rigorously.

Bibliography

[1] Philip W Anderson. "Absence of diffusion in certain random lattices". In: *Physical review* 109.5 (1958), p. 1492.

[2] Ad Lagendijk et al. "Fifty years of Anderson localization". In: *Physics today* 62.8 (2009), pp. 24–29.

[3] Hefei Hu et al. "Localization of ultrasound in a three-dimensional elastic network". In: *Nature Physics* 4.12 (2008), pp. 945–948.

[4] Mordechai Segev et al. "Anderson localization of light". In: *Nature Photonics* 7.3 (2013), pp. 197–204.

[5] Ragi Abou-Chacra et al. "A selfconsistent theory of localization". In: *Journal of Physics C: Solid State Physics* 6.10 (1973), p. 1734.

[6] Giulio Biroli et al. "Anderson model on Bethe lattices: density of states, localization properties and isolated eigenvalue". In: *Progress of Theoretical Physics Supplement* 184 (2010), pp. 187–199.

[7] Andrea De Luca et al. "Anderson localization on the Bethe lattice: Nonergodicity of extended states". In: *Physical review letters* 113.4 (2014), p. 046806.

[8] Giulio Biroli and Marco Tarzia. "Delocalization and ergodicity of the Anderson model on Bethe lattices". In: *arXiv preprint arXiv:1810.07545* (2018).

[9] Marc Mézard and Giorgio Parisi. "The cavity method at zero temperature". In: *Journal of Statistical Physics* 111 (2003), pp. 1–34.

[10] Marc Mézard and Riccardo Zecchina. "Random k-satisfiability problem: From an analytic solution to an efficient algorithm". In: *Physical Review E* 66.5 (2002), p. 056126.

[11] Marcel Filoche and Svitlana Mayboroda. "Universal mechanism for Anderson and weak localization". In: *Proceedings of the National Academy of Sciences* 109.37 (2012), pp. 14761–14766.

[12] Marcel Filoche et al. "Anderson mobility edge as a percolation transition". In: *Physical Review B* 109.22 (2024), p. L220202.

[13] B. Bollobás. *Random Graphs (2nd ed.)* Cambridge University Press, 2001.

[14] Nicholas C Wormald et al. "Models of random regular graphs". In: *London mathematical society lecture note series* (1999), pp. 239–298.

[15] F. Evers and A. D. Mirlin. "Anderson transitions". In: *Rev. Mod. Phys.* 80 (2008), p. 1355.

[16] Marc Mezard and Andrea Montanari. *Information, physics, and computation*. Oxford University Press, 2009.

[17] EN Economou and Morrel H Cohen. "Existence of mobility edges in Anderson's model for random lattices". In: *Physical Review B* 5.8 (1972), p. 2931.

[18] Tommaso Rizzo and Marco Tarzia. "Localized phase of the Anderson model on the Bethe lattice". In: *Physical Review B* 110.18 (2024), p. 184210.

[19] Dietrich Stauffer and Ammon Aharony. *Introduction to percolation theory*. Taylor & Francis, 2018.

[20] Bopeng Zhang et al. "The trade-off between membrane permselectivity and conductivity: A percolation simulation of mass transport". In: *Journal of Membrane Science* 597 (2020), p. 117751.

[21] Bong June Sung and Arun Yethiraj. "Lateral diffusion and percolation in membranes". In: *Physical review letters* 96.22 (2006), p. 228103.

[22] Lauren Meyers. "Contact network epidemiology: Bond percolation applied to infectious disease prediction and control". In: *Bulletin of the American Mathematical Society* 44.1 (2007), pp. 63–86.

[23] LM Sander et al. "Percolation on heterogeneous networks as a model for epidemics". In: *Mathematical biosciences* 180.1-2 (2002), pp. 293–305.

[24] Marcel Filoche et al. "Localization landscape theory of disorder in semiconductors. I. Theory and modeling". In: *Physical Review B* 95.14 (2017), p. 144204.

[25] Abel Klein. "Extended states in the Anderson model on the Bethe lattice". In: *Advances in Mathematics* 133.1 (1998), pp. 163–184.

[26] Michael Aizenman et al. "Stability of the absolutely continuous spectrum of random Schrödinger operators on tree graphs". In: *Probability theory and related fields* 136 (2006), pp. 363–394.

[27] Douglas N Arnold et al. "Effective confining potential of quantum states in disordered media". In: *Physical review letters* 116.5 (2016), p. 056602.

[28] Vito AR Susca et al. "Cavity and replica methods for the spectral density of sparse symmetric random matrices". In: *SciPost Physics Lecture Notes* (2021), p. 033.

[29] Giorgio Parisi et al. "Anderson transition on the Bethe lattice: an approach with real energies". In: *Journal of Physics A: Mathematical and Theoretical* 53.1 (2019), p. 014003.

[30] KS Tikhonov and AD Mirlin. "Critical behavior at the localization transition on random regular graphs". In: *Physical Review B* 99.21 (2019), p. 214202.

[31] Alexander Kraskov et al. "Estimating mutual information". In: *Physical Review E—Statistical, Nonlinear, and Soft Matter Physics* 69.6 (2004), p. 066138.

[32] Marc Mézard and Giorgio Parisi. "The Bethe lattice spin glass revisited". In: *The European Physical Journal B-Condensed Matter and Complex Systems* 20 (2001), pp. 217–233.

Appendix A

Discrete limit

We can easily recover Eq. (1.28) from Eq. (1.29) in the case of an hyper-cubic lattice in d-dimensions by writing the spatial derivatives of $f(\mathbf{x})$ as:

$$\frac{\partial f}{\partial x_\alpha} \approx \frac{f(\mathbf{x}+\mathbf{e}_\alpha) - f(\mathbf{x})}{1}, \tag{A.1}$$

$$\frac{\partial^2 f}{\partial x_\alpha^2} \approx \frac{f(\mathbf{x}+\mathbf{e}_\alpha) + f(\mathbf{x}-\mathbf{e}_\alpha) - 2f(\mathbf{x})}{1^2}. \tag{A.2}$$

Here we have taken the lattice constant equal to 1. Now the first term of Eq. (1.29) becomes:

$$\begin{aligned}
&-\frac{t}{u^2}\nabla\cdot(u^2\nabla\varphi) = -t\sum_{\alpha=1}^{d}\left(\frac{2}{u}\frac{\partial u}{\partial x_\alpha}\frac{\partial \varphi}{\partial x_\alpha} + \frac{\partial^2\varphi}{\partial x_\alpha^2}\right) = \\
&= -t\sum_{\alpha=1}^{d}\left[\frac{2}{u(\mathbf{x})}\Big(u(\mathbf{x}+\mathbf{e}_\alpha) - u(\mathbf{x})\Big)\Big(\varphi(\mathbf{x}+\mathbf{e}_\alpha) - \varphi(\mathbf{x})\Big) + \varphi(\mathbf{x}+\mathbf{e}_\alpha) + \varphi(\mathbf{x}-\mathbf{e}_\alpha) - 2\varphi(\mathbf{x})\right] = \\
&= -\frac{t}{2}\sum_{j\in\partial i}\left[\frac{2}{u_i}(u_j-u_i)(\varphi_j-\varphi_i) + 2(\varphi_j-\varphi_i)\right] = \\
&= -t\sum_{j\in\partial i}\frac{u_j}{u_i}(\varphi_j-\varphi_i).
\end{aligned} \tag{A.3}$$

In the third line we have used that for an hyper-cubic lattice the nearest neighbors of a site in position $\mathbf{x}$ are positioned in $\mathbf{x}\pm\mathbf{e}_{\mathbf{ff}}$ for $\alpha = 1,\ldots,d$.

Appendix B

Green's function chain rules

In this section we summarize the main steps to derive the chain rules of Eqs. (2.19). As for the derivation of Sec. 2.1, we use the cavity method. To compute the quantity $\mathcal{G}_{0r} = \langle 0|\hat{\mathcal{G}}|r\rangle$, where 0 and r are two sites in the Bethe lattice at distance r, we start from Eq. (2.1), writing

$$\mathcal{G}_{0r} = \frac{1}{Z}\int \mathcal{D}x\, x_0 x_r e^{-S_0[x]}\,. \tag{B.1}$$

After integrating out all the variables that are not on the unique simple path on the lattice connecting site 0 and site r, the integral can be written in terms of the normal and cavity marginals of Eqs. (2.6),(2.7), that in absence of the field J read

$$\mu_i(x_i) \propto e^{-\frac{x_i^2}{2\mathcal{G}_{ii}}}\,, \tag{B.2}$$

$$\mu_{i\to j}(x_i) \propto e^{-\frac{x_i^2}{2\mathcal{G}_{i\to j}}}\,. \tag{B.3}$$

Thus, we have

$$\begin{aligned}
\mathcal{G}_{0r} &= \int \prod_{s=0}^{r-1} [\mathrm{d}x_s\, \mu_{s\to s+1}(x_s)]\, dx_r\, \mu_r(x_r) x_0 x_r e^{t\sum_{s=0}^{r-1} x_s x_{s+1}} \\
&= \int \prod_{s=1}^{r-1} [\mathrm{d}x_s\, \mu_{s\to s+1}(x_s)]\, dx_r\, \mu_r(x_r)(t\mathcal{G}_{0\to 1}x_1) x_r e^{t\sum_{s=1}^{r-1} x_s x_{s+1}} \\
&= t\mathcal{G}_{0\to 1}\mathcal{G}_{1r} = \cdots = \left[\prod_{s=0}^{r-1} t\mathcal{G}_{s\to s+1}\right]\mathcal{G}_{rr}\,.
\end{aligned} \tag{B.4}$$

Here in the second line we have explicitly computed the Gaussian integral

$$\int dx_0 \mu_{0\to 1}(x_0) e^{t x_0 x_1} = t\mathcal{G}_{0\to 1}x_1\,. \tag{B.5}$$

In the last line we have just repeated the same integration procedure for all s.

The other version of the chain rule can be obtained in an analogous way by using the latter formula to compute the matrix element $\mathcal{G}_{r0}$, and by noticing that $\mathcal{G}_{ij} = \mathcal{G}_{ji}$.

Appendix C

Algebraic steps in the derivation with u alone

Starting from Eq. (2.18) we use Eqs. (2.19) to write

$$\begin{aligned}
&\mathcal{G}_{ik} = t\mathcal{G}_{i\to k}\mathcal{G}_{kk}, \\
&\mathcal{G}_{ij} = \mathcal{G}_{jj}\prod_{(s,s')\in p_{ij}} t\mathcal{G}_{s\to s'} = t\mathcal{G}_{i\to k}\underbrace{\mathcal{G}_{jj}\prod_{(s,s')\in p_{kj}} t\mathcal{G}_{s\to s'}}_{\mathcal{G}_{kj}} = t\mathcal{G}_{i\to k}\mathcal{G}_{kj},
\end{aligned}$$

where $p_{ij} \equiv \{\text{directed path connecting site } i \text{ and site } j\}$. Plugging these into Eq. (2.17) we immediately obtain Eq. (2.20) This solution is equivalent to the one of Sec. 2.1.1, in fact if we take

$$u_{i\to j} = \mathcal{G}_{ii}\eta_{i\to j}, \tag{C.1}$$

we obtain again the recursive Eqs. (2.20):

$$u_i = \mathcal{G}_{ii}\eta_i = \mathcal{G}_{ii} + t\sum_{k\in\partial i}\mathcal{G}_{ii}\eta_{k\to i}\mathcal{G}_{k\to i} = \mathcal{G}_{ii} + t\sum_{k\in\partial i}\mathcal{G}_{i\to k}u_{k\to i}\,, \tag{C.2}$$

$$u_{i\to j} = \mathcal{G}_{ii}\eta_{i\to j} = \mathcal{G}_{ii} + t\sum_{k\in\partial i\setminus j}\mathcal{G}_{ii}\eta_{k\to i}\mathcal{G}_{k\to i} = \mathcal{G}_{ii} + t\sum_{k\in\partial i\setminus j}\mathcal{G}_{i\to k}u_{k\to i}\,. \tag{C.3}$$

Here the second equalities in the two equations follow from Eqs. (2.19), indeed,

$$\mathcal{G}_{ii}t\mathcal{G}_{k\to i}\eta_{k\to i} = \mathcal{G}_{ik}\eta_{k\to i} = \mathcal{G}_{kk}t\mathcal{G}_{i\to k}\eta_{k\to i} = t\mathcal{G}_{i\to k}u_{k\to i}\,. \tag{C.4}$$

Conversely, it is easy to check that by defining $\eta_i = u_i/\mathcal{G}_{ii}$ and $\eta_{i\to j} = u_{i\to j}/\mathcal{G}_{ii}$ we can recover Eqs. (2.14) from Eqs. (2.20).

Appendix D

Population dynamics algorithm

The population dynamics algorithm is a method used to solve self-consistent distributional equations. It is accurately described in the context of message-passing algorithms on random graphical models in Ref. [16]. Here, we present a modified version of the algorithm, which has also been used to solve the Bethe lattice spin-glass problem in Ref. [32].

Consider a Bethe lattice with connectivity $K+1$ and the cavity equation that relates a cavity variable X to K independent copies of itself on the nearest neighboring sites $\{X_k\}_{k=1,\dots,K}$, along with a random variable drawn from a distribution γ:

$$X = \Psi\left(\{X_k\}_{k=1,\dots,K}; Y\right). \tag{D.1}$$

It is important to note that the variables in this equation are not necessarily scalars. For example, in the set of cavity equations given by Eqs. (2.12), (2.14), and the equation on the right in (2.27), we will have $X = (\mathcal{G}_{i\to j}, \eta_{i\to j}, \bar{p}_{i\to j})$, and $\{X_k\}_{k=1,\dots,K} = \{\mathcal{G}_{k\to i}, \eta_{k\to i}, \bar{p}_{k\to i}\}_{k=1,\dots,K}$.

We aim to find the probability distribution P such that, when $\{X_k\}_{k=1,\dots,K}$ are independent random variables drawn from P, the equality in Eq. (D.1) holds in distribution. This means P is the solution to the equation

$$P(x) = \int dy\, \gamma(y) \left[\prod_{k=1}^{K} dx_k\, P(x_k)\right] \delta\Big(x - \Psi\left(\{x_k\}_{k=1,\dots,K}; y\right)\Big). \tag{D.2}$$

The algorithm is based on defining a "pool" (or "population") of N variables $\{X_i\}_{i=1,\dots,N}$, each initialized independently by drawing from an initial distribution. We select an integer T as the number of iterations. The empirical distribution of $\{X_i^{(t)}\}_{i=1,\dots,N}$ at iteration t is denoted $\tilde{P}^{(t)}$. At each iteration step t, we sample a variable $y^{(t)}$ from γ and randomly select $K+1$ indices $\{i_0,\dots,i_K\}$ from $\{1,\dots,N\}$. We then replace $X_{i_0}^{(t-1)}$ in the population with

$$X_{i_0}^{(t)} = \Psi\left(\{X_{i_k}^{(t-1)}\}_{k=1,\dots,K}; y^{(t)}\right), \tag{D.3}$$

while keeping all other variables unchanged.

Assuming Eq. (D.2) has a solution, it can be argued that for sufficiently large T and N, the empirical distribution $\tilde{P}^{(T)}$ will be a good approximation of P.

Appendix E

Numerical evaluations through Montecarlo sampling from $P(g,\eta)$

In this appendix we summarize the method that we have used to compute numerically many of the quantities related to the localization landscape percolation. All the following procedures have in common that they involve the sampling of pairs of cavity Green's functions and cavity rescaled fields from the $P(g,\eta)$ that solves

$$P(g,\eta) = \int d\varepsilon\, \gamma(\varepsilon) \left[\prod_{k=1}^{K} dg_k d\eta_k\, P(g_k,\eta_k)\right] \delta\left(g - \frac{1}{\varepsilon - t^2 \sum_k g_k}\right) \delta\left(\eta - 1 - t\sum_k g_k \eta_k\right). \tag{E.1}$$

$P(g,\eta)$ is computed via population dynamics (App. D). As argued at the end of Sec. 3, with a negligible error we can substitute $P(g,\eta)$ with the product $P_g(g)P_\eta(\eta)$ where the marginal distributions $P_g(g)$ and $P_\eta(\eta)$ are the ones derived in Sec. 3.1. This avoids repeated population dynamics simulations when varying W. Numerically, we found that the Pearson correlation coefficient $r \sim O(10^{-2})$ and the mutual information is of $O(10^{-2}\text{bits})$ for the parameter ranges that we used, confirming that the approximation in Eq. (3.15) introduces negligible errors.

E.1 Computation of q and $\bar{q}$

The occupation probability q for the localization landscape percolation problem can be written as

$$q = \Pr\{O_i = 1\} = \mathbb{E}[O_i]\,, \tag{E.2}$$

and it can be computed explicitly through Montecarlo sampling:

$$q = \frac{1}{M}\sum_{m=1}^{M} O_i^{(m)}\,, \tag{E.3}$$

where for each sample m we draw $\{\mathcal{G}_{k\to i}^{(m)}, \eta_{k\to i}^{(m)}\}_{k\in\partial i\setminus j}$ from from $P(g,\eta)$ to compute the occupation variable $O_i^{(m)}$. Alternatively, having the analytical expression of the marginal distribution of $u_{i\to j}$ (see Eq. (3.20)), in the high connectivity limit we can just compute $q = \int du\, P_u(u)\theta(u - 1/E)$.

The conditional probability $\bar{q}$ from Eq. (3.42) can be computed by rewriting it as

$$\bar{q} = \frac{\Pr\{O_{k\to i} = 1, O_{i\to j} = 1\}}{\Pr\{O_{i\to j} = 1\}} = \frac{\mathbb{E}[O_{k\to i}O_{i\to j}]}{\mathbb{E}[O_{i\to j}]}\,. \tag{E.4}$$

Again, the expectation values of this expression can be evaluated using Montecarlo sampling, i.e.

$$\bar{q} = \frac{\sum_{m=1}^{M} O_{i\to j}^{(m)} O_{k\to i}^{(m)}}{\sum_{m=1}^{M} O_{i\to j}^{(m)}} \stackrel{d}{=} \frac{1}{K} \frac{\sum_{m=1}^{M} O_{i\to j}^{(m)} \sum_{k\in\partial i\setminus j} O_{k\to i}^{(m)}}{\sum_{m=1}^{M} O_{i\to j}^{(m)}}, \tag{E.5}$$

where for each of the M samples, $\{\mathcal{G}_{k\to i}^{(m)}, \eta_{k\to i}^{(m)}\}_{k\in\partial i\setminus j}$ are drawn from $P(g,\eta)$ to compute the occupation variables $O_{i\to j}^{(m)}$ and $\{O_{k\to i}^{(m)}\}_{k\in\partial i}$ (defined from Eq. (3.40)). The last equality in Eq. (E.5) follows from the statistical equivalence of the variables $\{O_{k\to i}\}_{k\in\partial i}$.

E.2 Computation of $C_p(r)$ and S

From the definition of correlation function in Eq. (1.16), by taking all bonds as active, and for a given distance r, one can write

$$C_p(r) = \Pr\{O_0 = 1, \ldots, O_r = 1\} = \mathbb{E}\left[\prod_{s=0}^{r} O_s\right], \tag{E.6}$$

thus,

$$C_p(r) = \frac{1}{M} \sum_{m=1}^{M} \prod_{s=0}^{r} O_s^{(m)}, \tag{E.7}$$

where the O_s are the ones defined in Eq. (1.12), and the occupation condition for a site s is $u_s > 1/E$. Each u_s is computed in terms of the on-site Green's function and the rescaled field as $u_s = \mathcal{G}_{ss}\eta_s$, where $\mathcal{G}_{ss}$ and η_s are computed as functions of their cavity counterparts on the nearest-neighboring sites of the path between site 0 and site r (i.e. $\{(\mathcal{G}_{k\to i}, \eta_{k\to i}) \,|\, i \in \{0,\ldots,r\}, k \in \partial\{0,\ldots,r\}\}$) according to Eq. (2.12) and equation on the right in (2.14). Thus, in order to compute a sample of $\prod_{s=0}^{r} O_s^{(m)}$, we just need to draw $K(r+1)+2$ iid pairs of cavity Green's functions and cavity rescaled fields from $P(g,\eta)$. The correlation length of $C_p(r)$ is evaluated by fitting the functional form $e^{-r/\xi_p}/K^r$ to the curve $C_p(r)$ in the non-percolating phase, computed for $r \gg 1$.

For the computation of S we just use the definition in Eq. (1.17). Therefore, we need to compute the correlation function $C_p(r)$ up to a cutoff distance r_{max} and perform explicitly the sum in Eq. (1.17).